Interfering with Calcium Release Suppresses I_γ, the "Hump" Component of Intramembranous Charge Movement in Skeletal Muscle

L. CSERNOCH, G. PIZARRO, I. URIBE, M. RODRÍGUEZ, and E. RÍOS

From the Department of Physiology, Rush University School of Medicine, Chicago, Illinois 60612

ABSTRACT   Four manifestations of excitation–contraction (E–C) coupling were derived from measurements in cut skeletal muscle fibers of the frog, voltage clamped in a Vaseline-gap chamber: intramembranous charge movement currents, myoplasmic [Ca^{2+}] transients, flux of calcium release from the sarcoplasmic reticulum (SR), and the intrinsic optical transparency change that accompanies calcium release. In attempts to suppress Ca release by direct effects on the SR, three interventions were applied: (a) a conditioning pulse that causes calcium release and inhibits release in subsequent pulses by Ca-dependent inactivation; (b) a series of brief, large pulses, separated by long intervals (> 700 ms), which deplete Ca^{2+} in the SR; and (c) intracellular application of the release channel blocker ruthenium red. All these reduced calcium release flux. None was expected to affect directly the voltage sensor of the T-tubule; however, all of them reduced or eliminated a component of charge movement current with the following characteristics: (a) delayed onset, peaking 10–20 ms into the pulse; (b) current reversal during the pulse, with an inward phase after the outward peak; and (c) OFF transient of smaller magnitude than the ON, of variable polarity, and sometimes biphasic. When the total charge movement current had a visible hump, the positive phase of the current eliminated by the interventions agreed with the hump in timing and size. The component of charge movement current blocked by the interventions was greater and had a greater inward phase in slack fibers with high [EGTA] inside than in stretched fibers with no EGTA. Its amplitude at −40 mV was on average 0.26 A/F (SEM 0.03) in slack fibers.

The waveform of release flux determined from the Ca transients measured simultaneously with the membrane currents had, as described previously (Melzer, W., E. Ríos, and M. F. Schneider. 1984. *Biophysical Journal*. 45:637–641), an early peak followed by a descent to a steady level during the pulse. The time at which this peak occurred was highly correlated with the time to peak of the current suppressed, occurring on average 6.9 ms later (SEM 0.73 ms). The current suppressed by the above interventions in all cases had a time course similar to the time derivative of the release flux; specifically, the peak of the time derivative of release flux preceded the peak of the current suppressed by 0.7 ms (SEM 0.6 ms). The magnitude of the current blocked was highly correlated with the inhibitory effect of the interventions on Ca^{2+} release flux.

Application of tetracaine (20 μM) suppressed a component of charge movement with similar magnitude and kinetic properties a–c, and reduced or eliminated the effect of the conditioning pulse protocol. Thus, interventions a–c suppress the same component as 20 μM tetracaine, the "hump" of Q_γ current (I_γ). Since I_γ is blocked by interventions that interfere directly with release at the SR level, I_γ appears to be a consequence of calcium release. Several aspects of these results and results in the following papers suggest as a possibility that I_γ arises as Ca^{2+} binds to sites on the inner surface of the transverse tubule membrane, causing an increase in surface potential that drives additional intramembranous charge movement.

INTRODUCTION

The chemical processes that generate contractile tension in muscle are made possible by an increase in $[Ca^{2+}]$ in the myoplasm, due to the release of calcium stored in the sarcoplasmic reticulum (SR) through calcium channels of the SR membrane. These SR channels are operated by changes in the electric potential across the membrane of the transverse (T) tubules, continuous with the sarcolemma. Since the discovery of intramembranous charge movement (Schneider and Chandler, 1973) evidence has accumulated indicating that this current is generated as intramembrane proteins are altered by the electric field, and that this change in molecular conformation is an essential step in transducing the change in potential to channel opening. Thus, intramembrane charge movements have come to be considered direct manifestations of the voltage sensors of excitation–contraction (E–C) coupling.

However, many complexities of the charge movement became apparent as evidence accumulated associating charge movement with E–C coupling. In addition to a small, very fast component generated at Na channels (Vergara and Cahalan, 1978; Sizto, 1982), two major subdivisions appeared in the mobile charge of skeletal muscle membranes. Charge 1 and charge 2 are terms coined by Adrian and Almers (1976) to name charges that move in well-polarized (holding potential [h.p.] of −90 mV) and depolarized (h.p. of 0 mV) fibers, respectively. Additionally, the current of charge 1 usually shows a simple, approximately exponential component (I_β) and a slower hump-like component (I_γ; Adrian and Peres, 1977). Even though the measured phenomena are currents, it is customary to refer to charges, Q_β and Q_γ, the movement of which determines these currents. In this Greek letter terminology Q_α is synonymous with charge 2.

A recurrent problem in the studies of Q_γ is the lack of a unique definition or

method to separate the associated current, I_γ. One of the consequences of these studies is an alternative definition of I_γ. For descriptive purposes, in the present papers the main criterion is kinetic: I_γ is the hump component of charge movement current, when present.

I_γ is not always observed as a distinct kinetic phase (Melzer, Schneider, Simon, and Szűcs, 1986; Hollingworth, Marshall, and Robson, 1990). However, when it is visible, its correspondence with the phenomenon of Ca release is striking. In our experience, and as will be shown in these papers, it unfailingly appears at or slightly above the threshold voltage for release (or movement), it occurs earlier in time than the peak of the Ca transient (Csernoch, Huang, Szűcs, and Kovacs, 1988), and in general it has the properties that one would expect of a current directly gating the SR release channel. Due to this close correspondence, several authors have proposed that I_γ is carried by the voltage sensor of E–C coupling, and that I_β is the result of movement of another molecule, which may or may not also be required for the coupling function (reviewed by Huang, 1989).

In the present series of studies on single muscle fibers, intramembranous charge movement current and Ca transients are measured simultaneously, Ca release flux is derived from the Ca transients, and a number of interventions are carried out, primarily devised to interfere with the Ca release process. In principle, these interventions are not expected to affect the T membrane voltage sensor.

In this paper the interventions include a conditioning pulse shown to inhibit Ca release by Ca-dependent inactivation (Schneider and Simon, 1988), a pulse protocol that leads to Ca depletion in the SR (Schneider, Simon, and Szűcs, 1987), and an intracellularly applied Ca release channel blocker. All these interventions lead, unexpectedly, to the selective elimination of a delayed component of charge movement. When the records of total charge movement current exhibit a visible hump, the component suppressed coincides temporally with the hump and has a magnitude similar to the hump. Since these interventions should primarily affect the Ca release process, we conclude that I_γ accompanies Ca release as a consequence.

This component is then compared with that blocked by tetracaine, a classical definition of Q_γ, first used by Huang (1980) (cf. also Huang, 1981, 1982, and Hui, 1983a, b) and seen to be almost exactly the same as the current blocked by 20 μM tetracaine, a concentration of drug lower than that used in the classical definition.

The unexpected kinetic aspects of the suppressed current support a possible mechanism for its generation, suggested by W. K. Chandler (Horowicz and Schneider, 1981): an additional movement of capacitive charge as a consequence of binding of released Ca^{2+} to the intracellular face of the T membrane.

In the second paper (García, Pizarro, Ríos, and Stefani, 1991), the approach is to modify the Ca load in the SR by manipulating the concentration of Ca^{2+} and calcium buffers. These interventions eliminate a hump component with kinetics similar to the component uncovered in the first paper. The loss is reversed by reloading the SR.

In the third paper (Szűcs, Csernoch, Magyar, and Kovács, 1991) the drug caffeine, used often as a modifier of the properties of Ca release by the SR (Endo, 1975; Kovacs and Szűcs, 1983; Delay, Ribalet, and Vergara, 1986; Simon, Klein, and Schneider, 1989), is shown to alter Ca release and a hump component in the charge movement current in a way consistent with the interpretation that the hump is a

consequence of Ca release. Tetracaine (at 25 μM) is shown to have an effect on charge movement opposite that of caffeine. It is tentatively concluded that the primary site of action of low tetracaine is the SR release channel.

In the last paper (Pizarro, Csernoch, Uribe, Rodríguez, and Ríos, 1991) the hump component of intramembranous current is simulated quantitatively as a consequence of binding of calcium, coming from the SR, to fixed charges at or near the voltage sensors. This binding of Ca^{2+} modifies the transmembrane potential effective on the sensors, thereby causing additional charge movement.

Some of the present results have been published in abstract form (Csernoch, Pizarro, Uribe, Rodríguez, and Ríos, 1989).

METHODS

The experiments in this and the following papers were carried out in cut skeletal muscle fibers, singly dissected from the semitendinosus muscle of the common leopard frog *Rana pipiens* or the Southern leopard frog *Rana sphenocephala*, mounted in a double Vaseline-gap apparatus (or a single Vaseline-gap in the experiments of Szűcs et al., 1991). The fiber, under voltage clamp, was subjected to various patterns of pulse stimulation (methods for data acquisition and pulse generation described by Brum and Ríos, 1987), while two sets of measurements were carried out in parallel as described below.

Intramembranous Charge Movement Current

Intramembranous charge movement current was measured, in the presence of suitable impermeant ionic substitutes and channel blockers, as the difference between membrane capacitive currents during test and control pulses. The methods, which are slight modifications of those of Brum, Fitts, Pizarro, and Ríos (1988a) and Brum, Ríos, and Stefani (1988b), will be described below, incorporating the nomenclature of Hui and Chandler (1990) whenever possible. The voltage measured between one of the end pools and the center pool of the two-gap chamber ($V_1(t)$) was multiplied by a factor of 1.05 (to approximately offset gap measurement errors and cable decay), yielding an estimate of the membrane voltage in the working compartment, $V(t)$. Test pulses (usually 100 ms) were applied from the holding potential (-90 mV unless noted otherwise) and were sometimes preceded by a 100-ms prepulse to -70 mV. The purpose of the prepulse is to minimize the presence of charge 2 movements in the records, as discussed by Brum and Ríos (1987), and to reduce the proportion of I_β relative to I_γ. Positive-going 20-mV control pulses were applied from a -130- or -140-mV prepulse level, maintained for 200 ms. Normally, two control pulses followed every test. Currents, $\Delta I(t)$ were recorded during control and test (ΔI because the steady level preceding the pulse is subtracted before storage). The current records shown are unprocessed differences between test and scaled control currents:

$$\Delta I_a(t) = \Delta I_{test}(t) - [\Delta V_{test}/\Delta V_{control}] \, \Delta I_{control}(t) \tag{1}$$

where ΔV_{test} and $\Delta V_{control}$ are the differences between measured $V_m(t)$ before and during the last 90 ms of the (test and control) pulses. These differences, $\Delta I_a(t)$, are termed asymmetric currents and include capacitive as well as small ionic components. Fig. 1 *A* shows a family of such differences at various test voltages.

In a few cases the charge movement current, defined as the capacitive component in $\Delta I_a(t)$ and represented by $\Delta I_{cm}(t)$ (Hui and Chandler, 1990) was quantified. In these cases a sloping baseline was fitted to the ON portion of the asymmetric current record between the

51st and the 100th ms and another to the OFF portion between the 71st and the 145th ms. These baselines were subtracted from the ON and OFF portions of the record, respectively. The ON and OFF charges were then calculated as time integrals of the remaining current. No records with subtracted baselines are shown in this series of papers. When this correction procedure was used, the asymmetric currents $\Delta I_a(t)$ are shown with a superimposed baseline trace (Fig. 4).

Intervention-sensitive Currents

In many cases in the present papers the experiments consist of interventions that reduce (or increase) membrane current. In these cases, and especially when the interventions are rapid,
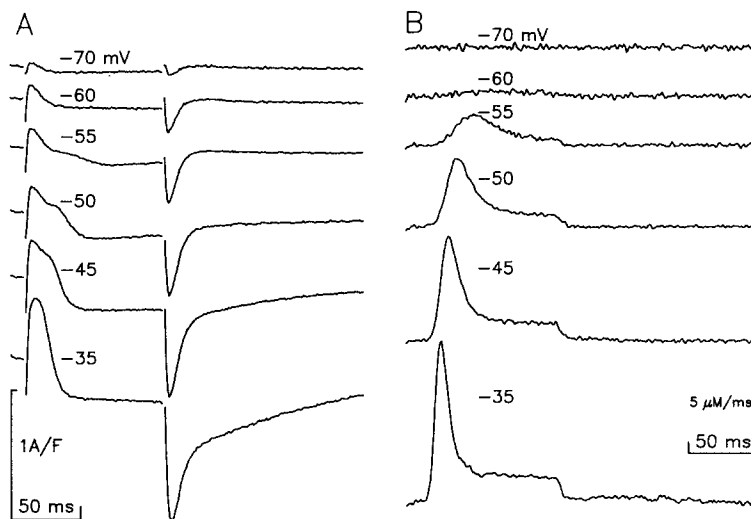

FIGURE 1. Asymmetric currents and Ca release flux in a stretched fiber. (*A*) Asymmetric currents $\Delta I_a(t)$ calculated as described in Methods. Test pluses from -90 mV (h.p.) to the voltages indicated. Control pulses: 20 mV from -130-mV prepulse level. Differences blanked for the first millisecond of ON and OFF transients. Records are averages of two sweeps obtained every 15 s. Controls are averages of four individual sweeps interspersed during the sequence. (*B*) Ca release fluxes $\dot{R}(t)$ derived from $[Ca^{2+}]_i(t)$ records of Fig. 2 with removal parameters listed in Table II. Fiber 496. External solution, Cd-La-A9C. Internal solution, reference. Linear capacitance, 12.5 nF. Diameter, 82 μm. Sarcomere length, 4 μm. Temperature, 14°C.

intervention-sensitive currents can be determined by direct subtraction of total currents during identical test pulses applied before and after the intervention. In most cases these difference currents have no fast transients, indicating that the linear capacitive current did not change. None of the interventions applied in these studies had reproducible effects on the fast capacitive current. In some cases the differences of total current had obvious fast components, but it was still possible to define an intervention-sensitive asymmetric current as the difference between $\Delta I_a(t)$ before and after the intervention. In this paper the following symbols are used to

represent the intervention-sensitive currents: $\Delta I_1(t)$, current suppressed by protocol 1; $\Delta I_2(t)$, current suppressed by protocol 2; $\Delta I_{rr}(t)$, current suppressed by ruthenium red; and $\Delta I_t(t)$, current suppressed by 20 μM tetracaine.

Ca^{2+} Transients

Ca^{2+} transients (time course of change in free myoplasmic calcium ion concentration) were derived from changes of optical absorption in the presence of the dye antipyrylazo III (ApIII) diffused intracellularly (methods described by Brum et al., 1988b). Briefly, wide-bandwidth light traversing the fiber was collected and split with a dichroic mirror centered at 780 nm. The two
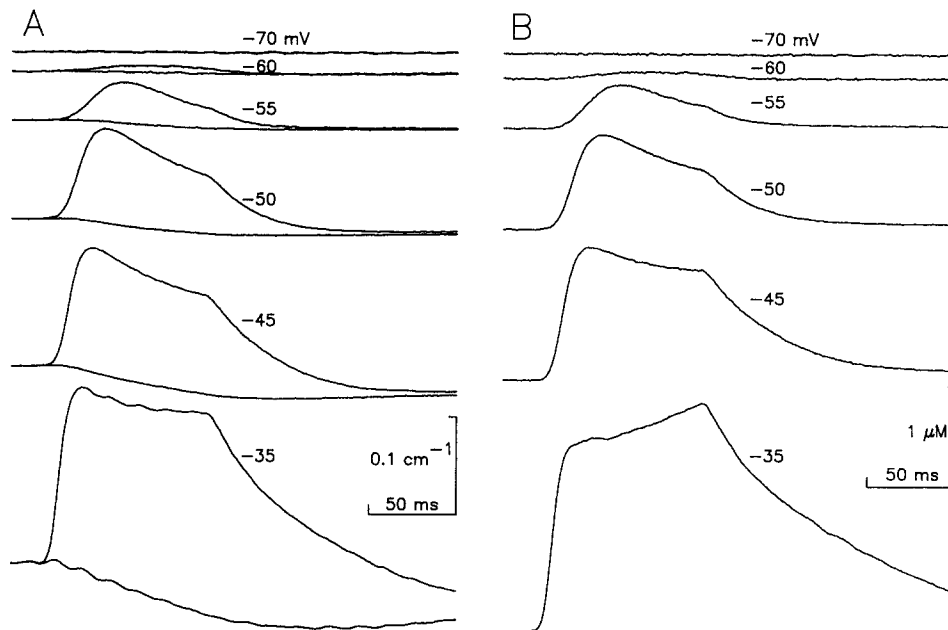

FIGURE 2. Optical signals and Ca^{2+} transients in a stretched fiber. (A) Absorbance changes at 720 nm (top traces in each pair) and at 850 nm (bottom traces) recorded simultaneously with currents in Fig. 1. (B) Changes $\Delta[Ca^{2+}]_i$ from the resting level, derived from the records in A. The ratio, intrinsic signal at 720 nm/intrinsic signal at 850 nm, was determined to be 1.3 at the beginning of the experiment. The complete sequence shown was obtained in 6 min, during which the dye concentration went from 612 to 683 μM.

beams were then trimmed by 50-nm bandwidth filters centered at 720 and 850 nm. Absorbance changes at these wavelengths, during pulses to various voltages that elicited the currents in Fig. 1 A, are represented in Fig. 2 A. The intrinsic absorbance change (recorded at 850 nm) was scaled using a factor that empirically matched the intrinsic absorbance change at 720 nm (determined at the beginning of every experiment, with no dye in the fiber). This scaled intrinsic signal was subtracted from the signal at 720 nm, yielding a calcium-dependent absorbance change. This waveform was then converted to change in calcium concentration ($\Delta[Ca^{2+}]_i(t)$) using the calibration data of Ríos and Schneider (1981) and Kovacs, Ríos, and Schneider (1983) and values of ApIII concentration obtained by linear interpolation from actual measurements of [ApIII] during the experiment. All the ApIII was assumed to be

capable of reacting with Ca^{2+}, the equilibrium was assumed to be instantaneous, and the affinity constant for Ca^{2+} at the temperature of the experiment was calculated by interpolation between the values given by Ríos and Schneider (1981) at 21°C and Kovacs et al. (1983) at 5°C after a correction for competition with the free Mg^{2+} present (Ríos and Schneider, 1981; Kovacs et al., 1983). Fig. 2 *B* shows the Ca transients corresponding to the absorbance changes in Fig. 2 *A*. This method can only determine *changes*, $\Delta[Ca^{2+}]_i$, from the resting level. When the actual $[Ca^{2+}]_i$ was needed (as in calculations of release flux) it was obtained by adding a resting $[Ca^{2+}]_i$

TABLE I

Solutions

	Internal		External			
	Reference	15EGTA	Reference	Co-Ca	10Ca	Cd-La-A9C
K	—	10	—	—	—	—
Na	14.5	28	—	—	—	—
Cs	121.2	80	—	—	—	—
Ca	8 μM		2	2	10	—
Mg	5.5	6.9	—	—	—	—
TEA	—	—	126	106.8	122.5	126
Cl	11	12.8	—	—	—	—
Glutamate	108	60	—	21.5	—	—
SO$_4$	—	—	—	21.5	—	—
CH$_3$SO$_3$	—	—	135	105.8	137.5	135.2
Tris maleate	17.7	—	5	5	5	5
EGTA	.1	15	—	—	—	—
ATP	5	5	—	—	—	—
Glucose	5	5	—	—	—	—
AP III	.8	.8	—	—	—	—
Mg^{2+}	.9	1.85	—	—	—	—
Ca^{2+}	50 nM	10 nM	2	2	10	*
Co	—	—	—	21.5	—	—
Cd	—	—	—	—	—	2
La	—	—	—	—	—	1
HEPES	—	10	—	—	—	—
Creatin phosphate	—	5	—	—	—	—
A9C‡	—	—	—	—	—	0.5

All concentrations in mM except where noted.
External solutions contained tetrodotoxin (1 μM) and 3,4 diaminopyrydine (1 mM).
*Contaminant Ca, (no Ca added).
‡A9C: anthracene-9-carboxylic acid.
Dissociation constants used. EGTA: Ca, 4.9×10^{-7} M. ATP: Mg, 9×10^{-5} M.
All solutions were titrated to pH 7.0.

to the monitored change. Resting $[Ca^{2+}]_i$ is assumed to be equal to $[Ca^{2+}]$ in the internal solution (50 nM in reference solution and 10 nM in the solutions with high [EGTA]). In most cases the changes recorded are in the micromolar range and the difference between $\Delta[Ca^{2+}]_i$ and $[Ca^{2+}]_i$ is negligible. Accordingly, the notation $[Ca^{2+}]_i$ is used throughout.

Flux of Calcium Release

The flux of calcium release from the SR ($\dot{R}(t)$) was derived from the Ca^{2+} transients by the technique of Melzer, Ríos, and Schneider (1987) as modified by Brum et al. (1988b). In this

technique several pulses of different durations and amplitudes, all of which cause Ca release, are applied, the corresponding absorbance transients are recorded, and the Ca^{2+} transients are computed as described. A quantitative model of Ca^{2+} removal from the myoplasm is then fitted simultaneously to the OFF portions of all Ca^{2+} transients. The removal model includes terms with the formal properties of all major Ca^{2+} binding and transport processes, including Ca^{2+} binding proteins, one of which exhibits competitive binding of Mg^{2+} and Ca^{2+}, binding and transport by the SR pump, and binding to foreign molecules, like EGTA and ApIII, that may be included in the internal solution. Since this model has many free parameters it is usually possible to obtain sets of their values that provide a very close fit to the experimental $Ca^{2+}(t)$. With the removal system described in this manner, a release flux waveform can be constructed from every Ca^{2+} transient as the sum of the removal flux and the time derivative of $[Ca^{2+}]_i(t)$ as described by Melzer et al. (1984, 1987). Fig. 1 B represents the records of $R(t)$ derived from the Ca^{2+} transients in Fig. 2, corresponding to the asymmetric currents in Fig. 1 A.

TABLE II

Parameters of Removal Model

Fiber No.	$k_{OFF,Mg,P}$	M	[P]	$k_{OFF,Ca,P}$	$K_{D,Pp}$	$k_{ON,Ca,P}$	$k_{ON,Mg,P}$	Temp.
	s^{-1}	s^{-1}	μM	s^{-1}	μM	$\mu M^{-1} s^-$	$\mu M^{-1} s^-$	$°C$
479	0.832	1340	150	1.0	1.0	100	0.03	14
482	7.28	599	614	1.0	2.0	100	0.03	13
483	5.20	1000	533	1.0	2.0	100	0.03	12.7
486	4.34	887	500	1.0	1.0	100	0.03	13
488	7.50	1505	539	1.33	1.49	100	0.03	13.2
489	1.36	756	513	1.0	2.0	100	0.03	14
490	9.70	739	702	0.95	0.85	165	0.04	13
492	5.15	500	289	0.84	1.52	100	0.03	13
496	9.40	700	540	0.73	0.62	68	0.03	13.5

Listed are those parameters in the removal model of Brum, Ríos, and Schneider (Brum et al., 1988a) that were allowed to change in the fit of at least one of the experiments tabulated. Symbols: K_D, dissociation constant. M, maximum pump rate. k_{ON}, binding rate constant. k_{OFF}, unbinding rate constant. P, parvalbumin. Pp, pump. T, troponin. Temp, temperature. Additional parameters, and their set values: $k_{OFF,Ca,T}$, 1200 s^{-1}. $k_{ON,Ca,T}$, 125 $\mu M^{-1} s^{-1}$. $[Ca^{2+}]$, 50 nM. [T], 240 μM. $[Mg^{2+}]$, 900 μM.

As demonstrated by Melzer et al. (1987), different methods of estimating the removal rates give similar waveforms of Ca release flux, provided that they describe well the decay of Ca^{2+} at the OFF of the transients. In other words, they are fairly insensitive to the structure of the removal model. Thus, and as argued by Brum et al. (1988b), fits of the removal model do not seem suitable to find "true values" of the parameters, different sets of values give comparably good fits. Thus, the fitting routines use literature values as starting points but are allowed to search freely in the positive set of rate constants and concentrations. The best-fit values of all parameters allowed to be changed by the fitting process and the set values of all others are listed for nine experiments on stretched fibers in Table II.

Solutions

Solutions were designed to eliminate ionic currents and avoid or minimize contractile movement of the preparation. For the first purpose, the internal solution was mostly Cs

glutamate and the external solution TEA methanesulfonate. The composition of the internal and external solutions is given in Table I. To avoid movement, two procedures were used. (*a*) In stretched fiber experiments the fibers were stretched beyond overlap of the myofilaments, usually 4.2–4.4 μm per sarcomere. (*b*) In slack fiber experiments EGTA was present in the internal solution at concentrations of 5, 8, or 15 mM (the 8-mM solution was obtained by mixing 5 EGTA and 15 EGTA). In these solutions with EGTA the nominal [Ca^{2+}] was 10 nM. All solutions had an osmolarity of 270 mosM and a pH of 7.0. The temperature was between 8° and 15°C and varied by less than 2°C during an experiment.

RESULTS

The results are the effects of four interventions on both asymmetric currents and Ca release flux. In all cases these are evaluated before and after the interventions. Figs. 1 and 2 illustrate basic phenomena in reference conditions. Fig. 1 *A* represents $\Delta I_a(t)$ records (Eq. 1) in a stretched fiber held at −90 mV and pulsed for 100 ms to the voltages indicated. Fig. 2 *A* represents the absorbance changes at 720 nm (top record in each pair) and at 850 nm, obtained simultaneously with the current records in Fig. 1. Fig. 2 *B* represents the Ca^{2+} transients derived from the absorbance changes in Fig. 2 *A*. As described in Methods, a removal model (Brum et al., 1988*b*) was fitted to all the records in Fig. 2 *B* and other records not shown. This model of removal was then used to determine the release flux underlying each Ca^{2+} transient (Melzer et al., 1984, 1987; Brum et al., 1988*b*). The resulting release flux waveforms, $R(t)$, are plotted in Fig. 1 *B*.

These figures illustrate two close associations. First, between the I_γ or hump component of the asymmetric current and the Ca release flux. A hump in the current is first clearly visible at −55 mV, which is also the voltage at which release becomes significant. At greater voltages the onset of release and the hump become much faster. The close agreement between the voltage at which I_γ was first seen and the threshold of release was a consistent finding. This observation will be made more quantitative later in this paper. Humps were found (either in ΔI_1 records or in intervention-sensitive currents) in 98 experiments. Ca release flux was monitored in 88 of these, either with the dye technique or through intrinsic absorbance changes. In all cases the presence of humps was accompanied by optical signals evidencing Ca release. We never observed humps without either intrinsic optical signals or Ca^{2+}-dependent dye signals. This was also true when high concentrations of EGTA were in the internal solution. The converse was not true; in some cases optical signals of Ca release were not accompanied by visible humps, and in rare cases no humps were present in the intervention-sensitive currents.

A second association exists between the Ca^{2+} transient and the intrinsic absorbance change (Hill, 1949; Barry and Carnay, 1969; Carnay and Barry, 1969; Kovacs and Schneider, 1977; Irving, Maylie, Sizto, and Chandler, 1987), as evidenced by the absorbance records in Fig. 2 *A*. This absorbance change, which is in most cases a decrease (increase in transparency), follows roughly the time course of the integral of [Ca^{2+}]$_i(t)$ (Ríos, Melzer, and Schneider, 1983). It is thus a slower phenomenon and its size can vary by orders of magnitude between experiments. Therefore, it constitutes an alternative monitor of Ca release (or increase in [Ca^{2+}]$_i$), although it is slower and

much less amenable to quantification. It is used in this paper in the experiments with ruthenium red, in which it was not possible to monitor $[Ca^{2+}]_i$ with ApIII.

Figs. 1 and 2 are representative of results obtained with stretched fibers with low intracellular EGTA. A similar set of records obtained with a slack fiber is presented in the second paper (García et al., 1991).

Our strategy was to apply interventions expected to reduce the magnitude of the Ca release flux from the SR as a primary effect. Recent work of Schneider and collaborators clarified the mechanism of two pulse protocols that reduce Ca release flux. A brief depolarizing pulse, itself activating maximal or near-maximal Ca release, depresses the ability to release in response to subsequent pulses. This depression appears to be due to two processes: (a) a Ca-induced inactivation of the release mechanism, which recovers in ~400 ms, and (b) transient depletion of Ca in the SR, which recovers in several seconds (Schneider, et al., 1987; Schneider and Simon, 1988). In addition to these negative effects of a previous depolarizing pulse, one expects that a prior depolarization would also cause voltage-dependent inactivation of the voltage sensor (Caputo, 1972). However, the onset time of voltage-dependent inactivation is ~2 s at 12°C (Brum et al., 1988a); therefore, depolarizations of 50 ms or less should not, in principle, alter the voltage sensor.

Protocol 1: Ca-dependent Inactivation

The above considerations suggested two pulse protocols that would alter Ca release flux in predictable ways. Fig. 3 shows an example of protocol 1, the application of a conditioning pulse of short duration (50 ms in the example) to a voltage that is suprathreshold for Ca release (−45 in the case represented) placed 150 ms before the test pulse. It causes Ca release (not shown) and has an inhibitory effect on the release accompanying the test pulse. The test pulse takes the membrane to a potential of −40 mV. The record labeled "reference" is the asymmetric current ΔI_a during the unconditioned test pulse. The presence of the conditioning pulse changes the ΔI_a ("conditioned"). When a hump is present (as in reference) it is either lost or reduced in the conditioned situation; the conditioned ΔI_a is always closer to a single exponential decay and this decay is usually slower than reference, as illustrated. The ΔI_a records shown were both constructed using the same control current; the third record is the intervention-sensitive current, that is, the result of subtracting the total current during the conditioned pulse from the current during the test pulse with no conditioning. (Since the ΔI_a records shown were constructed with the same control, the third record is also the difference between the reference and conditioned ΔI_a records).

The kinetic properties of the difference record are representative of the results of many experiments. They include: (a) a delayed onset, leading to a peak of outward current at 10–20 ms, followed by (b) a negative or inward phase, smaller and slower than the positive phase but seldom missing, and (c) a much smaller difference at the OFF, which in some cases was biphasic.

The next four figures compare the effects of a conditioning pulse on asymmetric current and Ca release flux. In three experiments the magnitude of the effects was changed by changing amplitude, duration, or placement of the conditioning pulse. Figs. 4 and 5 illustrate the effect of conditioning pulse amplitude. The large record

(reference) is the asymmetric current during a pulse to -40 mV (protocol in inset) in the absence of a conditioning pulse. The other records are differences between reference current and current during the test pulse in the presence of a conditioning pulse to the voltage indicated next to each record. The conditioning pulses to -65 and -55 mV have almost no effect, while the larger pulses suppress a current with the general characteristics shown in Fig. 3. (Note that in this particular fiber the membrane was taken to a large negative potential between conditioning and test. This procedure was intended to hasten recovery from any voltage-dependent inactivation, but it was later abandoned as it did not introduce obvious differences in
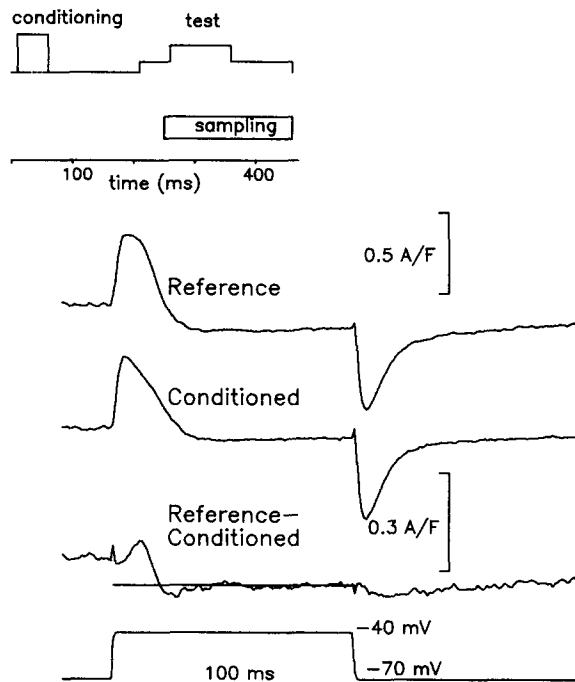

FIGURE 3. Example of protocol 1. Records labeled *Reference* and *Conditioned* are asymmetric currents elicited by a pulse to -40 mV. In *conditioned,* the test pulse was preceded by a 50-ms pulse to -45 mV. The detail of timing and test voltage is given schematically at the top. The test pulse rides on a prepulse to -70 mV installed 50 ms earlier. Record *reference-conditioned* was constructed by subtraction of total current during reference pulse minus total current during conditioned pulse. The same difference is found by subtraction of the asymmetric currents at top since the control was the same for both. At bottom is the voltage recorded, $V(t)$. Fiber 482. External solution, Cd-La-A9C. Internal solution, reference. Linear capacitance, 10.1 nF. Diameter, 83 μm. Sarcomere length, 4.0. Temperature, 13°C.

inactivation and caused large currents in the transition to the prepulse level, which in turn complicated the $\Delta I_1(t)$ records, as seen here.)

Fig. 5 shows records of Ca release flux derived from optical measurements in the same experiment, with the same pulse protocol but with a different sampling interval, which included the conditioning pulse as well as the test pulse. The record labeled "reference" is the release flux during a test pulse not proceded by a conditioning pulse. The other records show release during conditioning and test pulses, with conditioning pulses to the voltages indicated (the test voltage is always -40 mV). Qualitatively, the pulses to lower voltage caused smaller release and affected the test

release less, as expected from a Ca-dependent inactivation mechanism. As described by Schneider and Simon (1988), the effect on release during the test pulse is limited to the peak component of the release waveform, with little or no inhibition of the maintained component.

These aspects are presented quantitatively in Fig. 6. To obtain a measure of the effect on current, a baseline was fitted to the last 50 ms on the ON portion of the $\Delta I_1(t)$ currents in Fig 4 (baselines shown for three of the records) and subtracted. The difference record was integrated to obtain an ON charge suppressed by protocol 1 (O). An OFF charge was obtained in the same way (●). ON and OFF charges
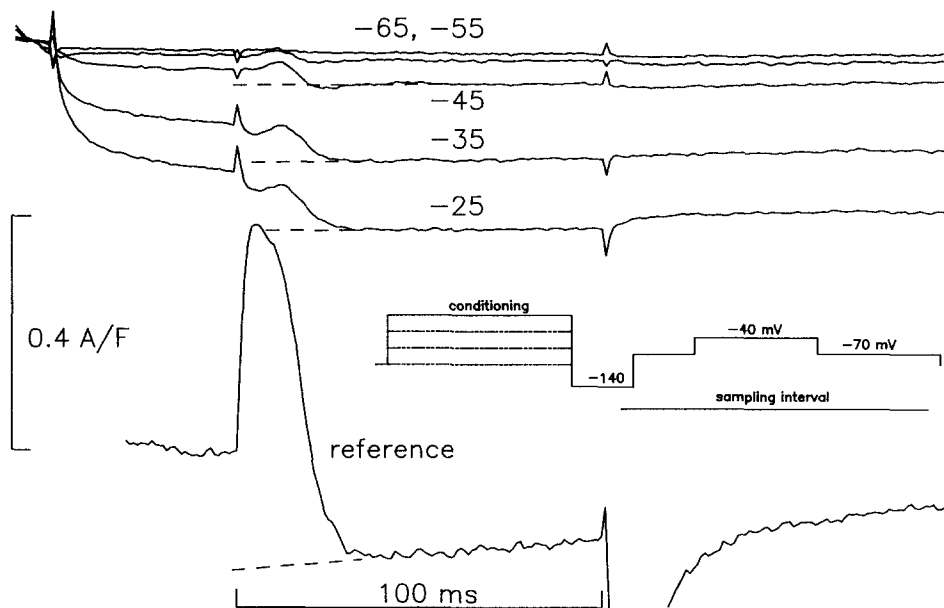

FIGURE 4. Effect of conditioning pulse voltage. (*Top*) Difference $\Delta I_1(t)$ between reference and conditioned currents elicited by a pulse to −40 mV. The conditioning protocol, of form C, is illustrated in the inset. The conditioning pulse voltage is indicated on the records. (*Bottom*) Reference asymmetric current, the common reference for all records at top. Dashed lines are baselines fitted to the records between 61 and 100 ms during the ON. The area of the reference transient after baseline subtraction was 16 nC/μF (ON) and 12.4 nC/μF (OFF). Fiber 482 (as in Fig. 3). Records are averages of two sweeps.

suppressed are plotted in Fig. 6 as a function of the conditioning pulse voltage. The ON charge suppressed increases sigmoidally with the conditioning pulse, while the OFF charge remains near zero. This discrepancy is an indication that the baseline subtraction does not provide a good reference line, either because it misses a small inward phase during the ON, or a small inward phase during the OFF, or both (the term "immobilization" could be used to describe the latter possibility). Thus, both ON and OFF areas are suspect as estimates of charge movement suppressed by protocol 1. The ON area as determined here, however, is a convenient measure of the magnitude of the effect. Another measure used later in this paper is the
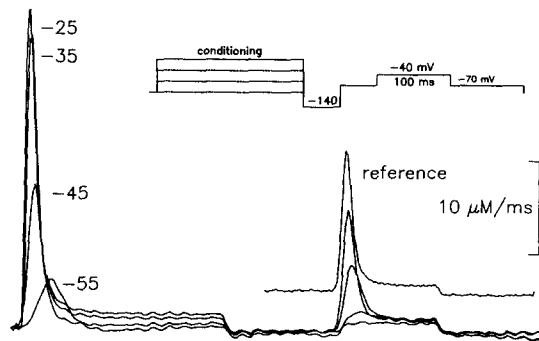
FIGURE 5. Effect of protocol 1 on release. Release records derived from Ca^{2+} transients elicited by protocol 1. Same fiber and voltages as in previous figure. Record labeled *reference* is obtained simultaneously with the corresponding record in Fig. 4. All others were obtained shortly after their homologous current records, as it was necessary to sample at a lower frequency to include the conditioning pulse. All records are single sweeps (except reference, which is an average of two sweeps) and were obtained in an 8-min interval, during which the dye went from 651 to 695 µM.

amplitude of the current suppressed. Its dependence on conditioning pulse voltage is similar to that of the ON area plotted in the figure.

Also plotted (open triangles) is the suppression of release, defined as the difference between peak Ca release flux in reference and conditioned test pulses. There is a rough proportionality between the ON charge suppressed and the release suppressed by the conditioning pulse. Finally, both variables are proportional to the peak value of release flux during the conditioning pulse, represented as open squares at half the scale of the suppression of release. A similar, rough proportionality exists with the final level of $\dot{R}(t)$ in the conditioning pulse.

In another experiment, illustrated in Fig. 7, the effect of a conditioning pulse was varied by changing the separation between conditioning and test pulses (protocol in inset). The effect on both ON charge and peak release flux were maximal at the shortest interval (50 ms) and decreased as the interval increased. The semilog plots in Fig. 7 are consistent with a roughly exponential time course of recovery, with time constants of 438 ms (for charge movement) and 426 ms (for Ca release flux). The similar time courses again indicate a very close correspondence between the effects of the conditioning pulse on release and charge movement.
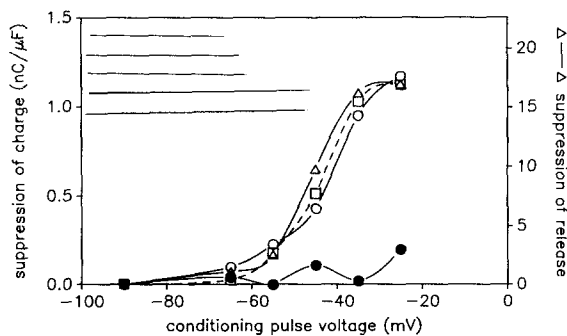

FIGURE 6. Effects of protocol 1 as a function of conditioning voltage. The plot collects the information from the previous three figures. ON (*open circles*) and OFF (*filled circles*) charges (integrals of records in Fig. 4 after baseline subtraction). *Triangles*, difference between peak release in reference and after a conditioning pulse (Fig. 5). When the conditioned release did not have a peak the maximum at the end of the pulse was used as subtrahend. *Squares*, Peak value of release flux during the conditioning pulse, divided by 2.

The effect of a conditioning pulse voltage was varied in another fiber by changing the duration of the pulse while keeping other parameters fixed. The longest pulse used (200 ms) caused the greatest affect on charge movement (ON charge suppressed was 3.5 nC/μF; OFF charge suppressed was 1 nC/μF) and Ca release flux (83% suppression of a 11.8 μM/ms peak value) elicited by a test pulse to -35 mV.

All experiments in which the parameters of the conditioning pulse were changed are summarized in Fig. 8, plotting fractional suppression of charge vs. fractional suppression of release flux. It can be seen that the correspondence between suppression of ON charge and release is good, regardless of the method used to change the effects.
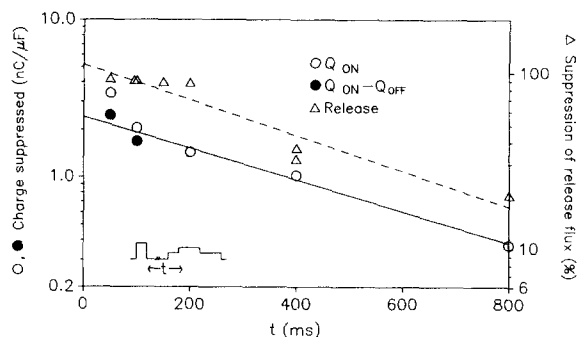

FIGURE 7. Effect of interval between conditioning and test. Dependence of release flux (*triangles*) and ON charge (*open circles*) as a function of the interval t between the end of the conditioning pulse and the beginning of the test (*inset*). Test pulse to -45 mV from prepulse level of -70 mV. Duration of test pulse, 100 ms. Conditioning pulse to -10 mV, duration 50 ms. Vertical scales are logarithmic. Charge suppressed is calculated as difference of a reference value (between 12.3 and 12.0 nC/μF from beginning to end of the sequence) minus a conditioned value. OFF values were also calculated but are small and were not plotted. The difference between the ON and OFF charges suppressed is plotted as filled circles for the only two values of t at which this subtraction makes a noticeable difference. The OFF value of the reference pulse was 9.6 and 10.6 nC/μF at beginning and end of the sequence. Linear capacitance, 7.98 and 7.88 nF, respectively. The release suppression is calculated as the difference between the peak value of a reference and the conditioned release, normalized to reference. Reference records were intercalated between conditioned records and their peaks varied between 5.63 and 3.02 μM/ms from beginning to end of the sequence. The sequence lasted 51 min, during which the dye concentration went from 920 to 1,190 μM. The first order regression lines drawn correspond to exponentials: 2.4 nC/μF exp ($-t$/438 ms) for suppression of charge, and 102 exp ($-t$/426 ms) for suppression of release. The two values of Q_{ON}-Q_{OFF} plotted were used instead of the values of Q_{ON} in the regression. Fiber 492. External solution Cd-La-A9C. Internal solution, reference. Diameter, 73 μm. Sarcomere length, 4.0 μm. Temperature, 13°C.

That the suppression is largely restricted to ON charge (open symbols) is also a consistent observation. Only the largest conditioning pulses at the closest intervals suppress some OFF charge (filled symbols). If the charge suppression at the OFF operated by a different mechanism, requiring large conditioning pulses of long duration placed close to the test pulse, it would be better to use the difference Q_{ON} − Q_{OFF} of charges suppressed as expression of the effect of protocol 1. This difference is plotted vs. release suppression in Fig. 8 B. The correlation coefficient for that plot is 0.929 and the regression line has a slope of 0.957 and an intercept of 0.012.

The general conclusion of this section is that the effect of a conditioning pulse on the asymmetric current (quantified here through the ON area of the current suppressed) is very well correlated with the reduction of peak release flux during the test pulse.

Ca release flux and the current suppressed by protocol 1 have an interesting kinetic relationship. As illustrated in Fig. 1, the hump component of charge movement current appears at the same potentials as Ca release flux and becomes faster together with release flux as the test potential increases. Since the current ΔI_1
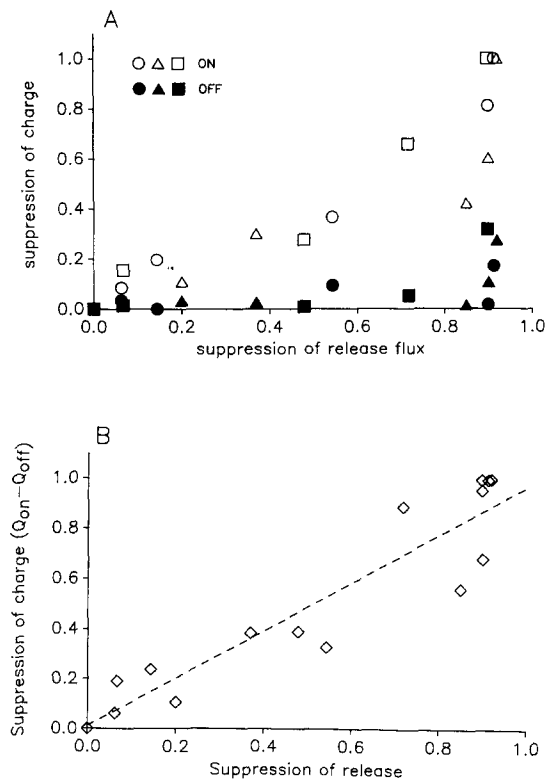

FIGURE 8. Correlation between the effects of protocol 1. (*A*) Relative suppression of charge by different conditioning pulses vs. suppression of release flux. Different symbols correspond to different experiments. Suppression of charge was normalized in every experiment to the maximum ON charge suppressed. The suppression of release was calculated as described for Fig. 6. Test pulse voltages are −40, −45, and −43 mV for fibers 482, 492, and 479, respectively. Prepulse levels: −70, −65, and −53 mV. Reference values of ON charge 9.49, 10.1, and 4.93 nC/μF. Linear capacitance: 9.89, 8.0, and 10.9 nF. Reference values of peak release: 13.8, 6.05, and 3.18 μM/ms. External solution for 479, Co-Ca. Other data in Table II and previous figures (*B*) Differences between ON and OFF values in *A*, normalized to individual maxima for each fiber. The first order regression line shown has slope 0.957 and intercept 0.012. The correlation coefficient is 0.929.

has a well-defined peak and in most cases a negative phase, it was possible to quantify its kinetics with two numbers, illustrated in the inset of Fig. 9: t_{m1}, the time to the positive maximum, and t_{01}, the time when ΔI_1 crosses the baseline fitted to the last 50 ms of the ON of $\Delta I_1(t)$. When $\Delta I_1(t)$ does not have a negative phase, as in two records of Fig. 4, t_{01} is not defined. Table III lists these parameters of ΔI_1 for different test pulses in a number of experiments in stretched fibers with reference internal solution. Additionally, the table lists the amplitude of the current suppressed, defined as the difference between the positive maximum and the minimum. In all cases the Ca transients were monitored optically and Ca release fluxes were derived. The time
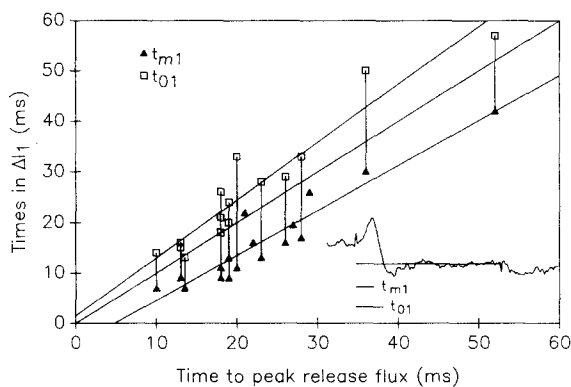
FIGURE 9. Kinetic comparison between release flux and $\Delta I_1(t)$. Time to peak of the current suppressed (*triangles*) and time to $\Delta I_1(t) = 0$ (*squares*) vs. time to peak release flux (t_{mR}). The times are defined in the inset. All values in Table III plus three additional values at high voltage from fibers 488 and 489 are plotted. Values from the same record are joined by a vertical line. The central line is $y = x$. The top line (first order regression of t_{01}) has slope 1.15 and intercept −1.51 ms. The bottom line (regression of t_{m1}) has slope 0.89 and intercept −4.3 ms. The correlation coefficients are 0.946 and 0.953, respectively.

TABLE III

Comparison of Kinetics of $\Delta I_1(t)$ and $\dot{R}(t)$

1 Fiber No.	2 V_{test}	3 ΔI_{m1}	4 t_{m1}	5 t_{01}	6 $\dot{R}_m$	7 $\dot{R}_{mc}$	8 t_{mR}	9 t_{mR}	10 8 − 4	11 9 − 4
	mV	A/F	ms	ms	μM/ms	μM/ms	ms	ms	ms	ms
483	−45	0.1	26	—	6.5	0.6	29	22	3	−4
	−35	0.1	16	—	10.5	1.15	22	16	6	0
	−25	0.17	11	—	11.3	1.20	18	12	7	1
488	−60	0.06	22	—	3.43	0.56	21	21	−1	−1
	−50	0.11	13	24	8.08	2.17	19	13	6	0
	−40	0.10	9	16	11.9	6.00	13	10	4	+1
	−30	0.10	9	15	13.9	—	13	9	4	0
489	−60	0.02	42	57	0.670	0.29	52	36	10	−6
	−50	0.07	30	50	2.19	0.72	36	25.5	6	−4.5
	−40	0.06	17	33	3.55	1.17	28	18	11	1
	−30	0.06	13	28	3.81	1.42	23	15	13	2
	−20	0.08	11	33	5.15	1.92	20	12	9	1
490	−35	0.13	11	26	14.4	2.64	18	9	7	−2
492	−45	0.17	11	18	5.10	1.07	18	11.5	7	0.5
	−25	0.15	7	13	9.40	2.44	13.5	7	6.5	0
496	−50	0.19	19.5	—	4.40	—	27	17	7.5	−2.5
497	−40	0.13	16	29	3.37	—	26	18	10	2
Avg.		0.14*	16.7	28.5			23.3	15.4	6.8	−0.68
SEM		0.015	2.19	3.92			2.34	1.85	0.80	0.57

Symbols: ΔI_{m1}, amplitude of current suppressed, from positive peak to negative minimum. t_{m1}, time to peak of ΔI_1, defined as in inset of Fig. 9. t_{01}, time to $\Delta I_1 = 0$, defined as in inset of Fig. 9. $\dot{R}_m$, maximum of release flux. $\dot{R}_{mc}$, maximum of conditioned release flux. t_{mR}, time to maximum of $R(t)$. t_{mR}, time to maximum of derivative of $\dot{R}(t)$. Parameters of the removal model used to compute release flux are in Table II.
*Only maximum values from each fiber used in this average.

to peak of release flux $(t_{m\dot{R}})$ is listed, as well as the peak release flux in reference and the maximum of the conditioned release flux.

Fig. 9 plots the characteristic times of ΔI_1 $(t_{m1}$, triangles; and t_{01}, squares) against the times to peak of $\dot{R}(t)$. In all cases $t_{m1} \leq t_{m\dot{R}} \leq t_{01}$. The times are highly correlated. The correlation coefficient of t_{01} and $t_{m\dot{R}}$ is 0.953 and that of t_{m1} and $t_{m\dot{R}}$ is 0.946. The regression lines (at top and bottom) have slopes of 1.15 and 0.89, respectively, for t_{01} and t_{m1}. From the averages in Table III the peak of $\Delta I_1(t)$ precedes the peak of $\dot{R}(t)$ by ~ 6 ms and $\Delta I_1(t)$ crosses the zero line some 5 ms after the peak of $\dot{R}(t)$.

Again, these correlations point at a close relationship between Ca release flux and the current suppressed by protocol 1, but the comparison in Fig. 10 reveals an unexpected aspect which will be central to our interpretation of this relationship. The
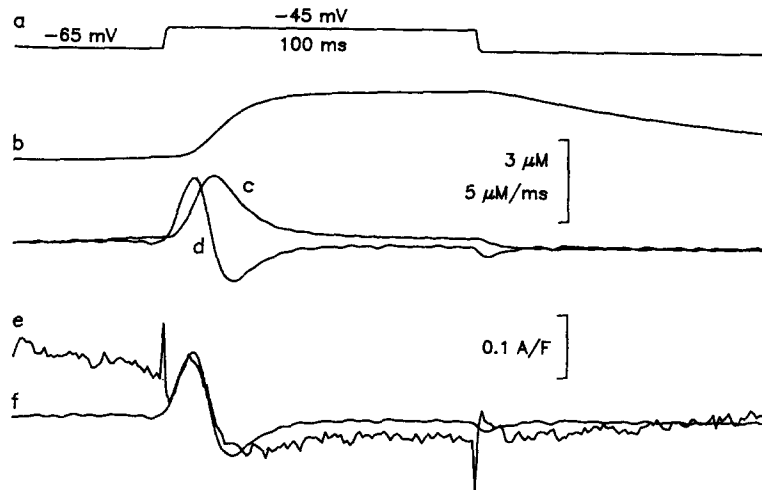

FIGURE 10. $\Delta I_1(t)$ and the first derivative of release flux. *a*, Voltage during test pulse; *b*, Ca^{2+} transients elicited by the pulse; *c*, release record $R(t)$ derived from *a*; *d*, time derivative of *c*, calculated as $\dot{R}_i = (R_{i+1} - R_{i-1})/2$. This calculation was then followed by a three point smoothing operation, $\dot{R}_i = (\dot{R}_{i-1} + 2\dot{R}_i + \dot{R}_{i+1})/4$. *e*, Current $\Delta I_1(t)$ suppressed by a conditioning pulse (to -10 mV, 50 ms, separated 200 ms from the beginning of the test pulse). *f*, Same as record *d*, shifted to match peaks with *e*. Fiber 492 (same as in Fig. 7). Dye at the time of the pulses, 920 μM. Other information in Table II.

top record in the figure is $V(t)$, going from a prepulse level of -65 mV to a test level $(-45$ mV) slightly suprathreshold for release (these records correspond to the 14th entry in Table III with ΔI_1 somewhat greater than average for the group). Record *b* is the Ca^{2+} transient elicited by the pulse. Record *c* is the release flux $R(t)$ derived from the Ca^{2+} transient (best fit parameters of the removal model given in Table II). Record *d* is the time derivative $(\dot{R}(t))$ of the release flux. Record *e* is the current $(\Delta I_1(t))$ suppressed by protocol 1. Record *f* is *d*, displaced vertically for comparison with ΔI_1.

$\Delta I_1(t)$ and $\dot{R}(t)$ have very similar kinetics, which is true of all cases studied (all entries in Table III, plus many records in nonstretched fibers, listed in Table IV). The parallel is especially good during the positive phase of $\Delta I_1(t)$; in general, the negative

phase of ΔI_1 is relatively smaller and slower, the negative minimum lagging the minimum of $\ddot{R}(t)$ by several milliseconds. Table III lists the times the peak of $\ddot{R}(t)$.[1] On average they are shorter than t_{m1} by 0.7 ms, an insignificant difference. Fig. 11 plots times to peak of $\ddot{R}(t)$ vs. t_{m1}. The correlation coefficient is 0.985 and the solid curve is the second order regression curve detailed in the figure legend.

This plot, Fig. 10, and the data in Table III demonstrate a strikingly parallel time course of $\Delta I_1(t)$ and $\ddot{R}(t)$. This parallelism is an important clue to the mechanism of the current $\Delta I_1(t)$. We will argue in the Discussion that local increase in $[Ca^{2+}]$ near the sites of release causes an increase in microscopic or local transmembrane potential and the movement of capacitive current. Since the time course of local $[Ca^{2+}]$ is expected to follow closely the time course of $\ddot{R}(t)$, additional capacitive

TABLE IV

Effect of Protocol 1 in Slack Fibers

Fiber No.	V_{test}	ΔI_{1m}	t_{m1}	t_{01}	External	Temp.	C_m
	(mV)	A/F	ms	ms	Solution	°C	nF
547	−40	0.06	13	—	Reference	9	9.90
549	−40	0.23	12	17	Co-Ca	12	19.9
550	−40	0.28	15	22	Co-Ca	12	22.2
558	−55	0.14	17	27	10 Ca	13	16.9
566	−55	0.17	13	19	10 Ca	14	11.7
567	−40	0.20	11	—	10 Ca	14	12.0
571	−30	0.27	11.5	18	Cd-La-A9C	12	9.88
572	−30	0.48	9	18	Cd-La-A9C	13	12.2
574	−20	0.28	14.5	25	Cd-La-A9C	13	7.63
612	−40	0.41	9	18	Reference	13	25.0
650	−50	0.24	12	22	10 Ca	14	32.2
651	−60	0.30	13	25	10 Ca	14	18.1
Avg.		0.26	12.5	21.1			
SEM		0.033	0.67	1.14			

The values tabulated are for the test potential (V_{test}) that resulted in the largest amplitude of $\Delta I_1(t)$. When two test potentials gave similar amplitude, the values for the lowest potential was included in the table. All fibers mounted at slack length. C_m, capacitance measured in the controls; other symbols as in Table III.

currents due to this hypothetical mechanism should follow $C \, dV_m/dt$, where V_m is the microscopic transmembrane potential and C is the appropriate capacitance. If, as elaborated later, the microscopic potential changes roughly proportionally to $R(t)$, $\Delta I_1(t)$ will roughly follow $\ddot{R}(t)$, as observed.

[1] In general the conditioning pulses used for protocol 1 were large and caused complete abolition of the peak of release. In these cases the derivative $\ddot{R}(t)$ was very similar to the derivative of the difference between reference and conditioned release fluxes. In a few cases the conditioned release was still high and we computed the derivative of the difference between reference and conditioned release for the purposes of the comparison in Table III. The time to the maximum of the derivative and the time course of its positive phase were very similar whether the derivative was computed from the reference release flux or the difference between reference and conditioned fluxes.

Similar studies of the effects of protocol 1 were carried out in slack fibers, with high EGTA in the internal solution. Amplitude and characteristic times of $\Delta I_1(t)$ in slack fibers are given in Table IV at the test voltage that makes the amplitude greatest. Initially we assumed that it would not be possible to monitor $[Ca^{2+}]_i$ optically in the presence of 15 mM EGTA, and we carried out a number of experiments without dye in the internal solution. (In later experiments we found it possible to monitor $[Ca^{2+}]_i$, and examples of Ca^{2+} transients and Ca release fluxes in high EGTA are given below.) Thus, Table IV does not have information on release flux comparable to that in stretched fibers. The records $\Delta I_1(t)$ were qualitatively similar in slack and stretched fibers, but the amplitude was greater in slack fibers, and the negative phase during the ON was more marked and present in all records. The average amplitude of the records in Table IV is 0.26 A/F, and the comparable average in stretched fibers (Table III) is 0.14 A/F. The difference is highly significant. The times t_{m1} and t_{01} are
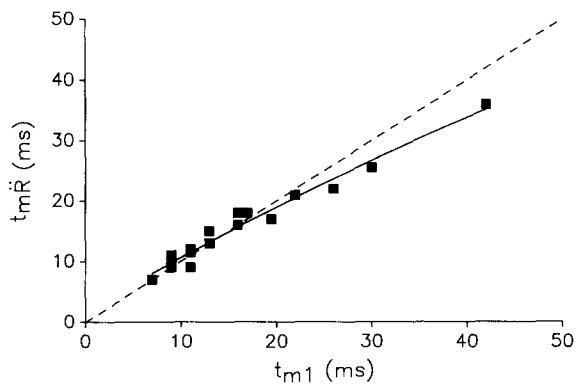

FIGURE 11. Kinetic comparison between $\Delta I_1(t)$ and derivative of release flux. Time to peak of $\dot{R}(t)$ ($t_{m\dot{R}}$) vs. time to peak of $\Delta I_1(t)$ (t_{m1}). Dashed line is $y = x$. Curve is the second order regression line of equation $y = 1.7$ ms $+ 0.92x + 0.003$ (ms^{-1}) x^2. The first order regression line, not shown, has slope 0.79 and intercept 2.83 ms. The correlation coefficients are 0.995 (second order) and 0.984 (first order). All values from Table III included, plus three additional values from fibers 488 and 489.

not significantly different in slack and stretched fibers. Examples of $\Delta I_1(t)$ records in slack fibers are given in Figs. 15, 17, and 18.

Another important aspect of the current defined by protocol 1 is its dependence on the voltage of the test pulse. The amplitude of the current, defined as in Table III, was found to go through a maximum at intermediate voltages and to decrease at higher voltages. An example of this observation is in Fig. 18. Other examples are given in the fourth paper of this series, where this voltage dependence is dealt with in detail. Given this voltage dependence, the tabulations in this paper are restricted to intermediate voltages (-60 to -20 mV).

Protocol 2: Depletion

The Ca-dependent inactivation of Ca release recovers with a time constant of $\simeq 100$ ms at 8°C (Schneider and Simon, 1988). Therefore, the reduction in release observed at intervals longer than 300 ms should be due to other mechanisms. In particular, Schneider et al. (1987) found evidence that it corresponds to Ca depletion in the SR

as Ca released by the conditioning pulse is transiently displaced to binding sites in the myoplasm. To maximize the depletion phenomenon and still not cause substantial voltage-dependent inactivation of the sensor or Ca-dependent inhibition of release channels, we devised the pulse protocol in Fig. 12, a "comb" of brief (50 ms; 20 ms in other cases) conditioning pulses, separated 700 ms or more from one another and from the test pulse (in order not to accumulate Ca-dependent inactivation).

Record a is the Ca release flux elicited by the test pulse when no conditioning pulses were applied. Record b is elicited by the test pulse after the depleting pulses. There is a reduction in size, again at the expense of the peak or inactivating phase of release (in other cases a greater reduction of the plateau level was also found). Record c is the direct difference between total membrane current in the reference condition and membrane current after the depleting comb, a difference we term $\Delta I_2(t)$. This difference is similar to the current suppressed by protocol 1, in both size
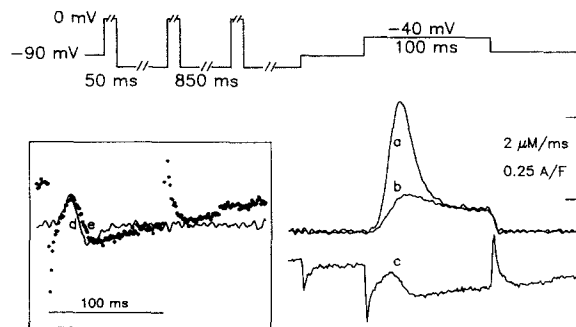

FIGURE 12. Protocol 2: depletion. (*Top*) Pulse protocol. a, Reference release flux derived from a Ca^{2+} transient (not shown); b, conditioned release flux after the depletion comb represented at top; c, current $\Delta I_2(t)$ suppressed by the conditioning protocol; d (*inset*), time derivative of the difference of release fluxes $(a - b)$ after three point smoothing as described in legend of Fig. 10; e, same as c, scaled to match peaks with d and shifted vertically. Fiber 479 (data in legend of Fig. 8 and Table III).

and kinetics (although in two of three experiments we observed the fast phases shown in the figure, with negative ON and positive OFF).

The depletion-sensitive difference $\Delta I_2(t)$ is replotted in the inset (e) for comparison with the derivative of the release flux suppressed by the comb. The agreement with the positive phase of $\dot{R}(t)$ is as good for $\Delta I_2(t)$ as it is for $\Delta I_1(t)$.

The results of three experiments on stretched fibers with this approach are summarized in Table V. The voltage of the test pulse was in all cases the one that made the effect on membrane current more visible, both in terms of magnitude and definition of the positive peak of the current $\Delta I_2(t)$. Neither amplitude nor time to peak of $\Delta I_2(t)$ were significantly different from the corresponding values of $\Delta I_1(t)$, and again the time t_{m2} to peak of $\Delta I_2(t)$ was very similar to the time to peak of the derivative of the release suppressed.

The conclusion from this section is that a depleting comb of brief depolarizations suppresses a current $\Delta I_2(t)$ similar to $\Delta I_1(t)$, and that the current suppressed is closely related to the time derivative of the release flux suppressed. A more radical approach to depletion is the topic of the second paper in this series.

Ruthenium Red

The effects of ruthenium red (RR) on E-C coupling have recently been summarized by Baylor, Hollingworth, and Marshall (1989). From their summary we repeat that RR blocks SR Ca^{2+} permeability in skinned fibers (Volpe, Salviati, and Chu, 1986) and in fractionated SR (Ohnishi, 1979; Miyamoto and Racker, 1982; Antoniu, Kim, Morii, and Ikemoto, 1985; Smith, Coronado and Meissner, 1985). It also blocks the channel activity of the ryanodine receptor reconstituted in lipid bilayers (Lai, Erickson, Rousseau, Liu, and Meissner, 1988) and ryanodine binding to this receptor (Pessah, Francini, Scales, Waterhouse, and Casida, 1986; Imagawa, Smith, Coronado, and Campbell, 1987). Finally, RR blocks the action potential–induced Ca transient when microinjected into intact fibers (Baylor et al., 1989). In a series of experiments illustrated in Figs. 13–16 and summarized in Table VI we examined the effect of

TABLE V

Effects of Protocol 2

1 Fiber No.	2 V_{test}	3 ΔI_{m2}	4 t_{m2}	5 t_{02}	6 $\dot{R}_m$	7 $\dot{R}_{mc}$	8 t_{mR}	9 t_{mR}	10 8 − 4	11 9 − 4
	mV	*A/F*	*ms*	*ms*	*μM/ms*	*μM/ms*	*ms*	*ms*	*ms*	*ms*
479	−40	0.17	13.5	—	13.9	8.65	21	13	7.5	−0.5
482	−45	0.09	8.5	—	6.05	2.89	15	9	6.5	0.5
492	−43	0.11	19	32	3.3	0.92	29	17	10	−2
Avg.		0.12	13.7				21.7	13.0	8.0	−0.67
SEM		0.029	3.71				4.97	2.82	1.27	0.887

Symbols: ΔI_{m2}, amplitude of current suppressed by protocol 2, from maximum to minimum. t_{m2}, time to maximum. t_{02}, time to $\Delta I_2(t) = 0$. Definition of both times illustrated in inset of Fig. 9. Other symbols as in Table III. External solutions: Co-Ca (479), Cd-La-A9C. Temperatures and removal parameters in Table II. All fibers were stretched (sarcomere lengths between 4.0 and 4.2 μm). Capacitance in the controls given for all fibers in legend of Fig. 8.

intracellular RR on intramembrane charge movement and E-C coupling and compared it with the effect of protocol 1.

In four experiments we attempted to diffuse RR into the fibers from their cut ends while monitoring Ca^{2+} transients with ApIII. In all cases the introduction of RR in the end pools together with ApIII resulted in the formation of a precipitate, and the condition of the fibers decayed rapidly. Additionally, and as reported by Baylor et al. 1989), RR both absorbs light at the wavelengths used in the ApIII technique and appears to bind the ApIII, eliminating its response in the presence of continued Ca release. For these reasons only experiments carried out without ApIII in the internal solution were successful. All the experiments with RR were carried out on slack fibers in view of the significantly greater amplitude of $\Delta I_1(t)$ obtained in this condition. Since we had to rely on the intrinsic absorbance change as sole monitor of release, and because this signal is generally small, and smaller in the presence of EGTA (Ríos, Brum, Pizarro, and Rodríguez, 1990), we used an external solution with 10 mM Ca^{2+}

as a device to increase release and charge 1, following the results of Brum et al. (1988a, b).

Fig. 13 illustrates results in one of three similar experiments in which the fibers before exposure to RR had both asymmetric currents with visible humps and measurable intrinsic absorbance signals upon stimulation. The fibers were first exposed to 5 mM EGTA internal solution (Table I) and several test and control pulses were applied to obtain reference ΔI_a records and absorbance records. The record labeled $-13'$ in Fig. 13 A was obtained 13 min before admission of RR in the
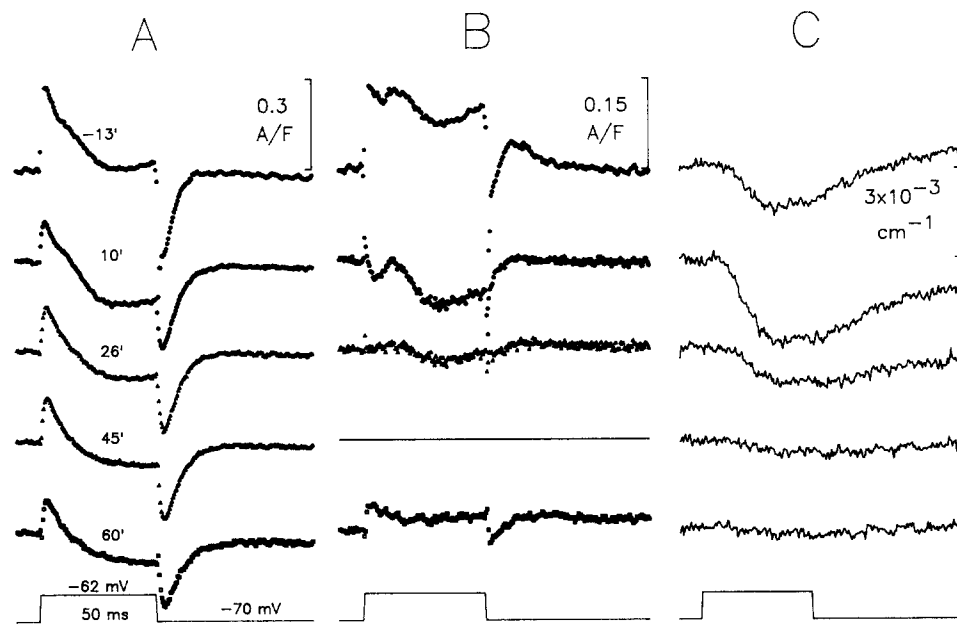

FIGURE 13. Effects of RR on current and intrinsic signal. (A) Asymmetric currents elicited by a pulse represented schematically at bottom. The pulse was applied at the times indicated next to each record. At time 0, an internal solution with 0.5 mM RR was substituted for internal solution 5 EGTA in the end pools. (B) Differences $\Delta I_\pi(t)$ between each record in A and the record at 45 min. (C) Intrinsic absorbance change at 850 nm, recorded simultaneously with test currents in A. All records except the one at 10 min are averages of two sweeps, one test and two control pulses per sweep, separated by 30 s. Record 10' is from a single sweep. Fiber 563. Diameter, 105 μm. Other data in Table VI.

end pools; the corresponding absorbance change is the first record in Fig. 13 C. With the fiber polarized at the holding potential, a solution with 0.5 mM RR was introduced in the end pools. The same test and control pulses were repeated afterwards at 15-min intervals. The successive ΔI_1 and absorbance records obtained are plotted in the figure, with the labels in A indicating time after admission of RR. At 10 min there were no major changes in asymmetric current (although the hump seems bigger) and the intrinsic signal increased about twofold. At later times the hump disappeared and the intrinsic signal became much smaller. B illustrates the

intervention-sensitive current $\Delta I_{rr}(t)$ obtained by subtracting $\Delta I_1(t)$ at 45 min, from the other records in A. In addition to fast components and shifts in level that were not reproducible, a delayed component in the early records is eliminated. This component has.the basic features of $\Delta I_1(t)$ and $\Delta I_2(t)$, including amplitude, characteristic times, and presence of two phases. Again the effects seem more important at the ON.

Fig. 14 summarizes the three experiments, represented by different symbols. The large symbols represent the amplitude (ΔI_{mrr}) of the RR-sensitive current $(\Delta I_{rr}(t))$, defined as the difference between total current at the times in the abscissa and total current at 50 min. The values for fiber 566 (triangles) were obtained differently, as explained below. Also, in two of these experiments the entry of RR was monitored by the change in resting absorbance in the fiber at 550 nm. From the change in absorbance and use of an extinction coefficient at 550 nm derived from the spectral curve given by Baylor et al. (1989), an average [RR] in the illuminated region was obtained and is represented by the small symbols.
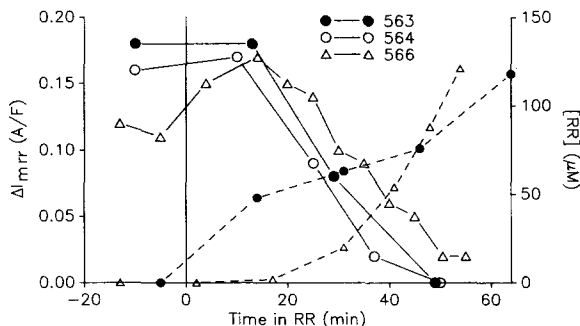
FIGURE 14. Summary of effects of RR on currents. *Large symbols*, Amplitude of $\Delta I_{rr}(t)$ (fibers 563 and 564) or $\Delta I_1(t)$ (566). *Small symbols*, Concentration of RR in myoplasmic water, calculated from the absorbance change at 550 nm, using $\epsilon(550) = 6.3 \times 10^4 \ M^{-1}s^{-1}$ (derived from the value at 530 nm, corrected by the ratio of absorbances at 550 and 530 nm measured in cuvette by Baylor et al. [1989]). The $\Delta I_{rr}(t)$ records were calculated for fibers 563 and 564 as differences between asymmetric currents at the time in the abscissa minus asymmetric current at the latest time plotted. For fiber 566 (*triangles*) the values plotted are amplitudes of $\Delta I_1(t)$ (records plotted in Fig. 15). External solution is 10 Ca in all cases. Internal solution is 5 EGTA. Slack fibers. Other data in Table VI.

In all cases the RR-sensitive current decreased with time of exposure after a lag, decaying to 50% in ~30 min. The properties of $\Delta I_{rr}(t)$ are given in Table VI. The amplitude (0.16 A/F) and characteristic times (13 and 21 ms) are similar to the corresponding average values for $\Delta I_1(t)$ and $\Delta I_2(t)$. Additionally, the table lists the time to the most prominent point of the visible hump in the asymmetric currents before exposure to RR (t_{mr}). This time is very similar to the time to peak of the RR-sensitive current, consistent with the impression that RR suppresses the hump.

The properties of $\Delta I_{rr}(t)$ and is association with the intrinsic absorbance signal are thus similar to the properties of the current ΔI_1 suppressed by protocol 1 and its association with Ca release flux. If both interventions suppress the same component of current, ΔI_1 will be reduced and eventually disappear in fibers exposed to RR. This prediction was confirmed by the experiment documented in Fig. 15. The records in A are the differences $\Delta I_1(t)$ induced by a conditioning pulse in the current determined by a pulse to -55 mV. The record labeled "reference" was obtained before exposure

TABLE VI

Effects of Ruthenium Red

Fiber No.	V_{test}	ΔI_{mrr}	t_{mrr}	t_{0rr}	t_{my}	C_m Reference	C_m RR	Temp.	Diameter
	mV	A/F	ms	ms	ms	nF	nF	°C	μm
563	−62	0.18	13	20	14	14.3	14.6	13.5	105
564	−60	0.16	14	26	15	21.3	24.1	*	108
566	−55	0.15	13	19	15	12.9	14.0	14°	89
Avg.		0.16	13.3		14.7				
SEM		0.01	0.4		0.4				

Symbols: ΔI_{mrr}, amplitude of current suppressed by ruthenium red (maximum-minimum). t_{mrr}, time to maximum. t_{0rr}, time to $\Delta I_{rr}(t) = 0$. t_{my}, time to most salient point of hump, determined by eye. C_m, capacitance in the controls. External solution, 10 Ca; internal, reference, 0.5 mM ruthenium red. All fibers mounted at slack length.

*Not measured, approximately 14°C (judged from power setting in cooling device).

to 0.5 mM RR in the end pools and the other records at the times indicated. The absorbance changes elicited by the test pulses are plotted in *B*. After an initial increase in both ΔI_1 and ΔA the two phenomena decay and disappear almost completely. The amplitudes represented by triangles in Fig. 14 are obtained from the records in *A* (as differences between maximum and minimum in each record) and
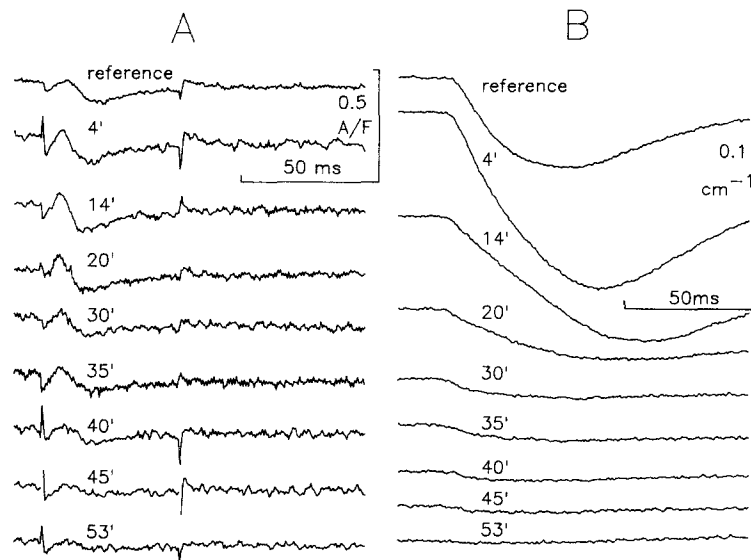

FIGURE 15. Protocol 1 and RR (*A*) $\Delta I_1(t)$ currents in a fiber exposed to RR. Pulse to −55 mV. Conditioning pulse to −30 mV, 50 ms duration, ended 200 ms before the beginning of the test pulse. Reference was obtained before exposure to RR as an average of four sweeps. Other records are from single sweeps at the indicated times after admission of RR in the end pools. (*B*) Absorbance changes at 850 nm, obtained simultaneously with the currents in *A*. Other data in Table VI.

thus are amplitudes of $\Delta I_1(t)$ currents rather than $\Delta I_n(t)$. $\Delta I_n(t)$ records were also constructed for this experiment. The amplitude decays with time very similarly to the amplitudes in Fig. 14. The similar size and kinetics of ΔI_n and ΔI_1, and the RR sensitivity of the latter, demonstrate that both interventions, a conditioning pulse and exposure to RR, affect the same component of intramembranous charge movement current.

The detailed measurements of ΔI_1 and ΔA in the experiment in Fig. 15 allowed us to estimate the concentration dependence of the effect. The amplitude of $\Delta I_1(t)$ (filled circles), the maximum value of $\Delta A_m(t)$ (triangles), and the average concentration of RR in the illuminated area of the fiber are plotted as a function of time in Fig. 16 A. In B the reciprocals of the current and absorbance amplitudes are plotted as a function of the concentration of RR. The points are close to the first order regression lines represented. The effect of RR in this particular fiber is therefore well described as a simple binding with first order dissociation constants of 11.4 μM (for current blocking) and 3.85 μM (for the intrinsic signal).

Effect of a Low Concentration of Tetracaine

In the previous sections we described three interventions or protocols that reveal a delayed component of intramembrane charge movement with several characteristic properties, present regardless of the procedure or intervention used. When a hump or I_γ component is present in the reference records, the hump is reduced or eliminated by the interventions. Thus the intervention-sensitive current can be identified with I_γ.

One classical definition of Q_γ is the portion of the charge movement suppressed by tetracaine (Huang, 1980; cf. also Huang, 1981a, 1982; Hui, 1983a, b; Vergara and Caputo, 1983; Csernoch et al., 1988; Huang and Peachey, 1989). To further characterize the current suppressed by the previous interventions, we compared it with the current suppressed by tetracaine. It was found that 20 μM tetracaine has effects on both current and $R(t)$ virtually identical to those of protocol 1 on both current and Ca release flux. This concentration of tetracaine is lower than the concentrations used in previous studies on intact fibers.

Fig. 17 A shows the effect of 20 μM tetracaine on asymmetric currents elicited in a slack fiber by pulses to two different voltages (recorded voltages at the bottom of B). The ΔI_a record at -40 mV (a) has a noticeable hump, followed by an inward-going phase during the ON (a common observation in slack fibers; cf. Pizarro et al. [1991]). Neither hump nor inward-going phase remain after 2 min in tetracaine (record b). The top record in B is the difference between total currents in reference and tetracaine; a similar record is obtained if asymmetric currents a and b are subtracted. The tetracaine-sensitive current (termed ΔI_t) has all the properties of the currents suppressed by the previous interventions.

The records at 0 mV illustrate the remarkable fact, already indicated for ΔI_1, that the magnitude of ΔI_t is greater at the lower voltage, comparing either amplitudes from maximum to minimum or areas of the initial positive phase at the ON. This was true in three experiments with this concentration of tetracaine. In two other experiments it was not possible to define the amplitude at 0 mV, either because it was
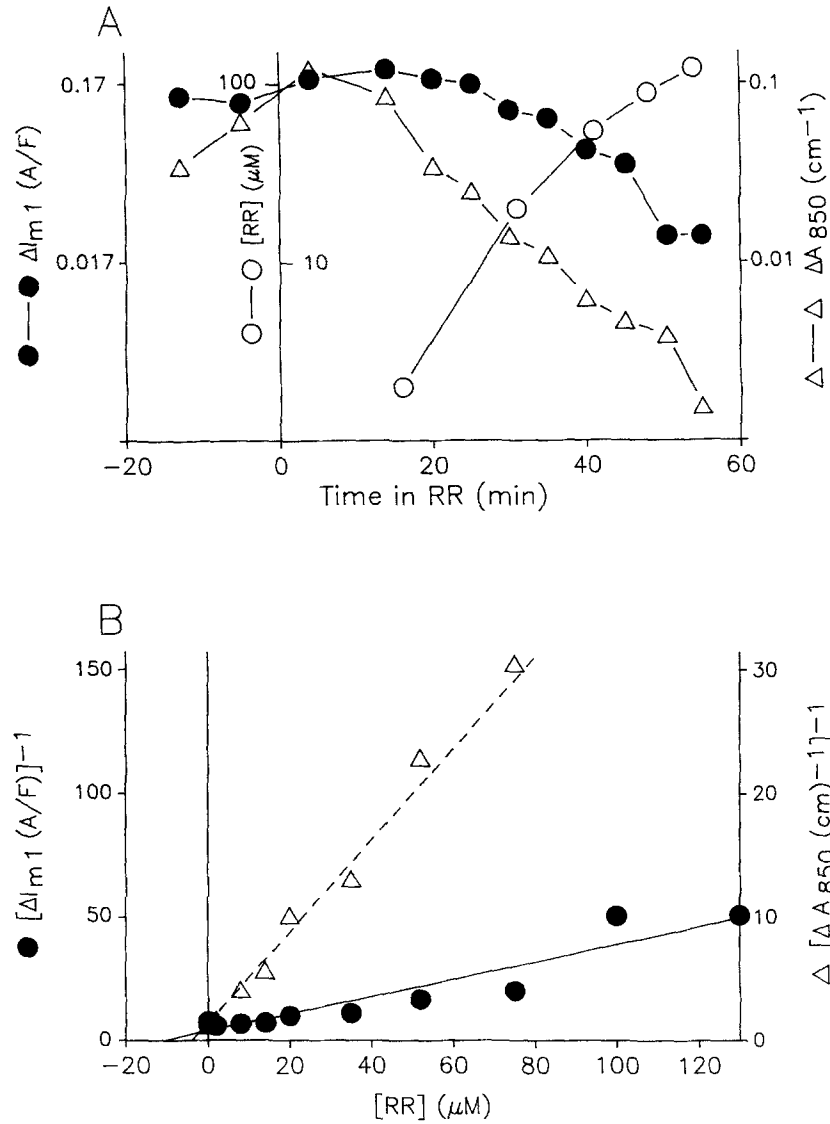
FIGURE 16. Concentration dependence of the effects of RR (A) ΔI_{m1} (amplitude of $\Delta I_1(t)$), calculated as difference between maximum and minimum of every record in Fig. 15 A (●) Peak value of ΔA_{850} (from Fig. 15 B) (△). Concentration of RR as a function of time after introduction of RR in end pools (○). Semilogarithmic scale. (B) Inverses of the amplitudes of $\Delta I_1(t)$ and $\Delta A_{850}(t)$ vs. [RR]. The first order regression lines intercept the abscissa at -11.4 μM (ΔI_1) and -3.85 μM (ΔA_{850}).

very small or because it occurred in the first 1 or 2 ms of the pulse, when our determinations of differences are rendered unreliable by large capacitive transients.

Fig. 18 illustrates the similarity between $\Delta I_t(t)$ and $\Delta I_1(t)$ obtained on the same fiber. The records in A are asymmetric currents obtained before tetracaine application both without (a and c) and with the conditioning pulse preceding the test pulse (b and d). The effect of the conditioning pulse on the asymmetric current is similar to the effect of tetracaine shown in Fig. 17. The records labeled $a - b$ and $c - d$ in panel B are the corresponding ΔI_1 records (differences between records in A). Immediately
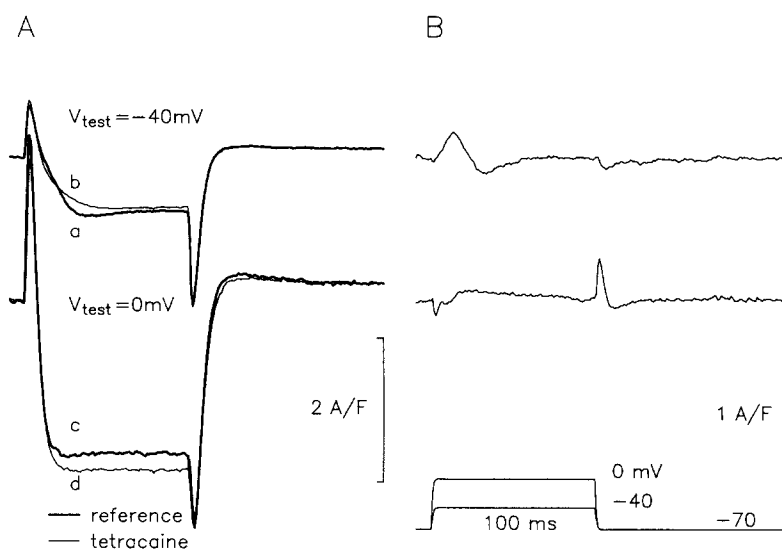

FIGURE 17. Effect of a low concentration of tetracaine on asymmetric current. (A) Records b and d, asymmetric currents elicited by pulses to -40 and 0 mV in the presence of 20 μM tetracaine in the external solution (voltage records in B). a and c, corresponding records in reference solution, introduced in the external compartment after tetracaine. The pulses were applied in the sequence d, b, a, c. Controls for d were obtained in tetracaine, for a, b, and c in reference. Very similar asymmetric currents result when an average of both controls is used. (B) Differences $\Delta I_t(t)$ between total currents (reference $-$ tetracaine). Fiber 550. Linear capacitance, 22.2 nF (in tetracaine) or 22.9 nF (in reference). Diameter not measured. Other data in Table IV.

after application of these protocol 1 pulses the fiber was exposed to tetracaine, and test pulses at both voltages were applied. The corresponding $\Delta I_t(t)$ records (which are similar to the ones shown in Fig. 17, obtained later in the same fiber) are plotted with thick lines in B. $\Delta I_t(t)$ and $\Delta I_1(t)$ are similar in magnitude and kinetics at both voltages.

Quantitative characteristics of the current ΔI_t at the lower voltage are listed in Table VII for five experiments in slack fibers. The average amplitude of the current
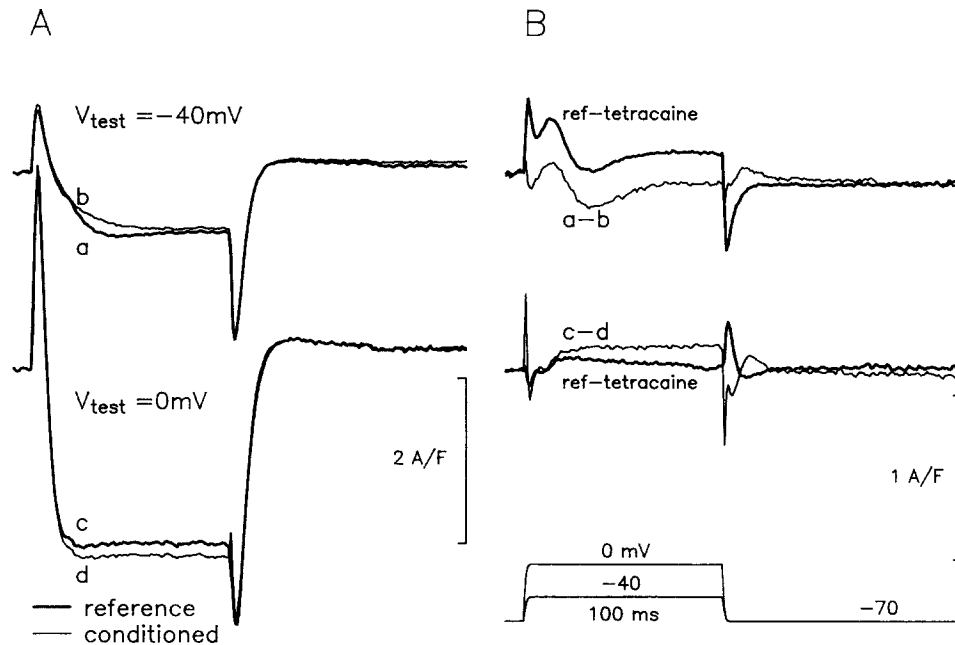
FIGURE 18. Tetracaine and protocol 1. (A) Asymmetric currents in reference solution. a and c elicited by pulses to the voltages indicated (records of $V(t)$ at bottom). b and d elicited by pulses preceded by a conditioning pulse (to 0 mV, 100 ms duration, terminating 400 ms before the test pulse). Controls are the same in both cases. (B) Differences $\Delta I_1(t)$ (*thin traces*) compared with tetracaine-induced differences in the same fiber. All current records in B are differences between total membrane currents. The reference record at -40 mV was obtained before tetracaine. The reference at 0 mV was obtained after washout. Same fiber as Fig. 17 (*ref-tetracaine* record at 0 mV is the same as the difference record at 0 mV in Fig. 17 B).

TABLE VII

Effects of 20 µM Tetracaine

Fiber No.	V_{test}	ΔI_{int}	t_{int}	t_{0t}
	mV	A/F	ms	ms
541	-55	0.22	13	19
547	-40	0.08	14.5	—
549	-45	0.25	11	18
550	-45	0.32	13	22
558	-55	0.18	17	28
Avg.		0.21	13.7	21.8
SEM		0.040	1.00	2.60

Symbols: ΔI_{int}, amplitude of current suppressed by 20 µM tetracaine, from maximum to minimum. t_{int}, time to maximum. t_{0t}, time to $\Delta I_t (t) = 0$. Additional information for all experiments except 541 in Table IV. Fiber 541. External solution, reference. Internal, reference, 3.6 µm/sarcomere. Diameter, 80 µm. Linear capacitance, 7.45 nF.

suppressed (0.19 A/F) is somewhat smaller than that of ΔI_1 in slack fibers (0.26 A/F; Table VI) and the characteristic times are very similar.

Results on stretched fibers also show a close similarity of ΔI_t and ΔI_1. In five experiments with stretched fibers we applied protocol 1 before and after exposure to 20 μM tetracaine and found that the amplitude of ΔI_1 decreased by 60–90%. Since tetracaine blocked a current similar to ΔI_1, it was expected that the effect of Ca release flux would also be similar. This was studied in stretched fibers, in which Ca^{2+} transients are not buffered and the release flux can be derived more precisely. Fig. 19 illustrates one of five experiments. In this fiber a pulse to −40 mV (bottom record) elicited Ca^{2+} transient f in reference conditions and g in the presence of tetracaine. The decay after the pulse of these and other transients could be fit with the same model parameters (as was the case for all experiments, suggesting that tetracaine at this concentration does not alter the removal processes). Records d and e are the corresponding Ca release fluxes. As was the case for protocol 1, the effect of this
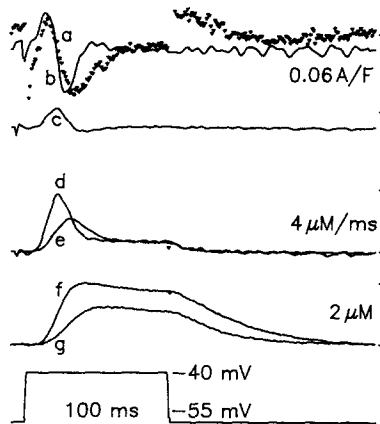

FIGURE 19. Tetracaine-sensitive current and $\dot{R}(t)$. *a*, Tetracaine-sensitive current moved by a pulse to −40 mV ($V_1(t)$ at bottom). *b*, Derivative of *c*, the release flux suppressed by tetracaine. *c* is calculated as the difference between *d* ($\dot{R}(t)$ before tetracaine) and *e* ($\dot{R}(t)$ in the presence of the drug). These flux records were derived from the corresponding Ca^{2+} transients *f* and *g* (parameters of removal in Table II described well the transients in reference and in tetracaine). The dye concentration was 346 μM. Fiber 486. External solution, Cd-La-A9C. Internal solution, reference, with all Cl⁻ replaced by glutamate. Diameter, 85 μm. Sarcomere length, 4.3 μm. Capacitance in controls, 12.8 nF (reference) or 12.4 nF (tetracaine).

concentration of tetracaine is restricted to the inactivating component of release flux, which in all cases was reduced in size and made slower, whereas the plateau was not visibly modified. Record *c* is the difference $d - e$ (the tetracaine-induced change in release flux) and *b* is its time derivative. Record *a* is the current $\Delta I_t(t)$ suppressed by tetracaine. The striking parallelism found between ΔI_1 and $\dot{R}(t)$ also exists between ΔI_t and the derivative of the tetracaine-suppressed release flux.

This block of results thus shows that 20 μM tetracaine inhibits essentially the same component of asymmetric current and release flux as protocol 1. As reported by Lamb (1986), concentrations of 0.4–4 mM tetracaine that served to define Q_γ in previous works resulted in rapid changes and deterioration of fibers. Studies in progress using intermediate concentrations reveal a greater inhibitory effect on release and suppress additional components of charge movement (Csernoch, L., G. Pizarro, I. Uribe, and E. Ríos, manuscript in preparation).

DISCUSSION

Four Interventions Inhibit Ca Release Flux

The first intervention used was a brief conditioning pulse to a potential high enough to elicit substantial Ca release. Schneider and Simon (1988) studied the mechanism of the inhibition of release caused by this protocol, concluding that the release process undergoes inactivation due to binding of Ca^{2+} to a site accessible from the myoplasm. This inactivation is also at work during a single pulse, explaining the spontaneous decay of release flux after the early peak during pulse depolarization. Schneider and Simon (1988) explained the voltage and time dependence of the inactivation, assuming that it requires a binding step followed by a slower inactivating conformational change. Such binding and inactivation probably occur at the release channel itself, mainly because reconstituted ryanodine receptor-Ca channels undergo Ca-dependent inactivation (Ma, Fill, Knudson, Campbell, and Coronado, 1988). It is thus reasonable to assume that through protocol 1 we are directly inhibiting Ca release flux at the release channel level.

The second intervention was designed to cause depletion of Ca in the SR. A comb of conditioning pulses as in Fig. 12, with 700 ms or more between pulses, should not build up Ca-dependent inactivation but cause depletion (Schneider et al., 1987). As shown in Fig. 12, the conditioned release waveform is indeed smaller. To qualify as a consequence of depletion only, this reduction should be a simple scaling of the reference waveform, without kinetic change (Schneider et al., 1987). The fact that the conditioned release waveform was slower, both in onset and relaxation after the peak, suggests that the conditioning also caused inactivation. Alternatively, since the test pulses are small and cause a small release, it is possible that the $[Ca^{2+}]_i$ reached during the conditioned pulse was not high enough to cause the maximum rate of Ca-dependent inactivation, thus explaining the slower kinetics of the conditioned release.

The smaller conditioned release was accompanied by a charge movement current lacking a small component of slow onset, $\Delta I_2(t)$. The kinetic properties of this component are similar to those of $\Delta I_1(t)$, the component suppressed by protocol 1. Thus both protocols, causing reduction of Ca release flux as primary effect, inhibit a component of charge movement with unusual properties. The attempt at depletion was only partially successful. A more radical approach to depletion is taken in the next paper, with greater effects, generally consistent with the present report.

The third intervention was the application of the release channel blocker RR. We had to omit ApIII and rely on the intrinsic signals to monitor the effect of RR on release. As expected, these signals consistently became smaller, then disappeared, 20–60 min after exposure to RR at the cut ends. A hump component was clear at intermediate depolarizations in all fibers before exposure to RR. In all cases this component decayed and ceased to be visible after 30–40 min in RR. By subtracting the asymmetric current remaining after 50 min in RR it was possible to define a RR-sensitive current and follow the time course of its disappearance. RR-sensitive current and intrinsic signal decayed more or less in parallel, with a similar time course in all experiments, including a lag of ≈ 15 min and a half-suppression time of ≈ 30 min. By contrast, untreated fibers usually give stable signals for hours. In sum,

RR inhibited Ca release flux and a component of charge movement current. Again, the primary target was probably the release channel.

Since all the interventions suppressed the hump in the asymmetric current, we compared their effects with those of tetracaine. Concentrations of tetracaine between 1 and 4 mM have been shown to suppress the hump component of charge movement in intact fibers (Huang, 1980, 1981, 1982; Hui, 1983*a*; Vergara and Caputo, 1983). We found that 400 μM tetracaine resulted in rapid deterioration in many fibers. In all cases a concentration of 20 μM was sufficient to significantly reduce Ca release flux and reduce or eliminate visible humps in the current. The inhibition of release was similar to the effect of the other interventions; specifically, the effect was restricted almost exclusively to the inactivating phase, without major changes in the plateau level.

The Interventions Suppress the Same Component of Asymmetric Current

The characteristics of the current suppressed by all four interventions are very similar. The kinetic properties include a distinct rising phase, a positive peak occurring at a time that depends strongly on pulse voltage and is ~15 ms near −50 mV, a negative phase visible in almost all cases, and an obvious asymmetry between ON and OFF, the OFF transient being generally smaller in amplitude and area, variable in polarity, and biphasic in many cases. When the currents suppressed by different interventions were determined in the same fiber (as $\Delta I_1(t)$ and $\Delta I_t(t)$ in Fig. 18, and $\Delta I_1(t)$ and $\Delta I_{rr}(t)$ in Fig. 15) they were virtually identical. When $\Delta I_1(t)$ was determined in fibers exposed to 20 μM tetracaine or after 30–40 min in RR, it was much smaller than in reference conditions. The average amplitude of the waveforms, measured from positive maximum to negative minimum were comparable (Tables III and IV for $\Delta I_1(t)$, Table V for $\Delta I_2(t)$, Table VI for $\Delta I_{rr}(t)$, Table VII for $\Delta I_t(t)$). It was difficult to quantify the current suppressed in terms of charge because of the presence of an inward phase during the ON. In many cases a baseline was clearly defined after the transient phases on the ON and the charge moving both in the outward and inward directions could be calculated (for instance, records in Figs. 3, 4, 10, 17, and perhaps 18). In these the outward component could carry as much as 7 nC/μF and the inward phase as much as 3.5 nC/μF. A detailed study of an inward phase in the asymmetric current is presented by Pizarro et al. (1991).

The Current Suppressed Is the Hump Component of Charge Movement

In the present experiments with stretched fibers, as well as in other works with similar techniques on stretched fibers (Brum et al., 1988*a*, *b*; Melzer et al., 1987), hump components are frequently absent or small (although large humps are found in occasional experiments, as in Fig. 1). By contrast, in the experiments on slack fibers described in this paper and the following papers in this series, I_γ is almost always visible and often large. Specifically, humps were visible in the asymmetric currents from all the fibers listed in Tables IV and VII. Visible humps were always significantly reduced or eliminated by the interventions described (examples for protocol 1 in Figs. 3 and 18, for RR in Fig. 13, for tetracaine in Fig. 17, and for all cases in Tables VII and IV). When a hump was not visible, the interventions still suppressed a current with the same characteristics, but with smaller amplitude. We conclude that these four

interventions specifically suppress or inhibit a component of charge movement that can be seen as a hump in the total asymmetric current, but may not be noticeable when it is small or too slow.

A Definition of I_γ

In previous works, Q_γ has been defined operationally in several ways: by its susceptibility to inactivation by changes in holding potential, by its delayed kinetics, and by its sensitivity to drugs, especially tetracaine. The peculiar delayed kinetics is Q_γ's most characteristic feature, so in this and the following papers we use the terms I_γ and hump component interchangeably. This does not constitute a quantitative definition because the baseline on which the hump rides is not defined. Hui (1983b) introduced a quantitative kinetic definition fitting the charge movement current with two terms of definite mathematical form, an exponential decay for I_β and a bell-shaped function for I_γ. This separation seemed reasonable and was apparently consistent with the observation that tetracaine removes the hump (Huang, 1981). It has shaped our thinking about I_γ to the extent that the mention of the term evokes images of bell-shaped current transients.

The separation of two additive terms proposed by Hui (1983b), however, is not the only possibility, and may not be adequate in view of the present results. We have shown that four interventions suppress the hump; however, in all cases the suppressed current has the hump component followed by a negative phase. Consistent with charge conservation, the OFF current suppressed is usually smaller, and the charge moved at the OFF is smaller than the charge moved in the positive phase of the ON. Thus, the interventions that suppress the hump do not suppress a component with the properties assumed in Hui's mathematical description. Based on the present observations, the mechanisms causing the hump also appear to cause important changes in kinetics after the hump. Specifically, these mechanisms also determine a rapid termination of the hump during the ON and sometimes cause the return of part of the charge after the hump; this amounts to a different kinetic description of I_γ. As we shall see, a model in which the hump is a consequence of Ca release flux naturally predicts the negative phase and smaller OFF currents. The possibility that I_γ includes other terms in addition to the intervention-sensitive current described here will be considered later.

The Effects on Charge and Ca Release Are Highly Correlated

The main purpose of this work is the comparison of effects of the interventions on charge movement with the effects on Ca release flux. The results show a close correspondence, in both magnitude and kinetics. Fig. 1 illustrates qualitatively a very precise relationship between the voltage dependence of Ca release and the occurrence of visible humps. Even though the threshold voltage for Ca release varied with the different external and internal solutions, we always found that the lowest voltages for noticeable humps were at or slightly above the threshold for release. We did not quantify this observation because the correspondence between current and release suppressed by various interventions lent itself better to precise quantification.

Consider first the close correspondence between the effects of protocol 1. As shown in Fig. 5, greater conditioning pulses suppress more of the peak of release during the test pulse and the suppression of release correlates well with the suppression of

charge in the test pulse. This is true whether the suppression of charge is estimated from an integral of the current suppressed (Figs. 4 and 6) or from the peak value of current suppressed. A similar close relationship was found when the degree of suppression was changed by changing the interval between conditioning and test pulses: both peak release and charge suppressed were greatest at the shortest intervals, and the suppression reversed as the interval increased, with approximately the same time constant (Fig. 7).

More striking are the kinetic correspondences between the current suppressed and the effect on release. As illustrated in Figs. 9–11, $\Delta I_1(t)$ is very close in time dependence to the derivative of release flux $\dot{R}(t)$. The correspondence includes an almost parallel time course of the positive phase, including close timing of their peaks, and it extends to the negative phase during the ON. The results of many experiments, summarized in Figs. 9 and 11 and Table III, indicate that the peak of release flux occurs ~7 ms later than the peak of I_γ, and 5 ms earlier than the time at which $I_\gamma(t)$ becomes negative. The peak of $\ddot{R}(t)$ occurs virtually at the same time as the peak of I_γ (0.7 ms earlier, on average). ApIII signals may lag the Ca^{2+} transient by 1.4 ms (Baylor, Quinta-Ferreira, and Hui, 1985). Tests (not shown) with lag-corrected Ca^{2+} transients showed that lags in the monitoring of $[Ca^{2+}]$ propagate unchanged to the estimate of release flux. Therefore, the peak of $\ddot{R}(t)$ measured with an instantaneously equilibrating dye would precede the peak of I_γ by $\simeq 2$ ms.

The close correspondence was present with three of the four interventions studied (it was not possible to determine release in the experiments with RR). This is shown in Figs. 9–11 for protocol 1, Fig. 12 for protocol 2, and Fig. 19 for tetracaine. That the correspondence was the same with all interventions is another indication that these affect the same component of charge movement.

Finally, the correspondence between I_γ, as defined by the present interventions, and the time derivative of release, extended to the negative phases in both waveforms. As can be seen in all the figures comparing these waveforms, the inward phase of I_γ lags several milliseconds behind the inward phase of $\ddot{R}(t)$ and in most cases has a proportionally smaller amplitude.

That the positive phase of I_γ corresponds so well to the positive phase of $\ddot{R}(t)$, a signal that has a negative phase, is an indication, albeit indirect, that the negative phase of I_γ has some relationship with E-C coupling. We argue below that this negative phase in the current is, as is the hump, a consequence of Ca^{2+} release.

I_γ as a Consequence of Ca Release

As we have seen, all interventions used here suppress or modify the hump component of charge movement current. Since the first three interventions presumably have the SR release process as primary target, the tentative conclusion from this work is that the current suppressed is a consequence of the release process.[2] The inward phase of the current suppressed should also be caused by the release process.

---

[2] We have started to explore the effects on single fibers of other drugs that block reconstituted ryanodine receptor/Ca channels. Octanol was found to block release and Q_γ but not Q_β when applied externally (González, Pizarro, Ma, Caputo, and Ríos, 1990). Ryanodine also had specific blocking effects on Q_γ (García, Avila-Sakar, and Stefani, 1991; and González, A., G. Pizarro, J. Ma, and E. Ríos, unpublished observations).

Another consequence of this work is that the effect of 20 μM tetracaine should also have the release process as primary target. Tetracaine is a well-characterized blocker of release in skinned fibers and fractionated SR, where it is more effective than procaine (Endo, 1985), and is a blocker of the Ca release channel reconstituted in bilayers (Xu et al., 1990). Observations in Szűcs et al. (1991) support the view that tetracaine primarily suppresses release at this low concentration.
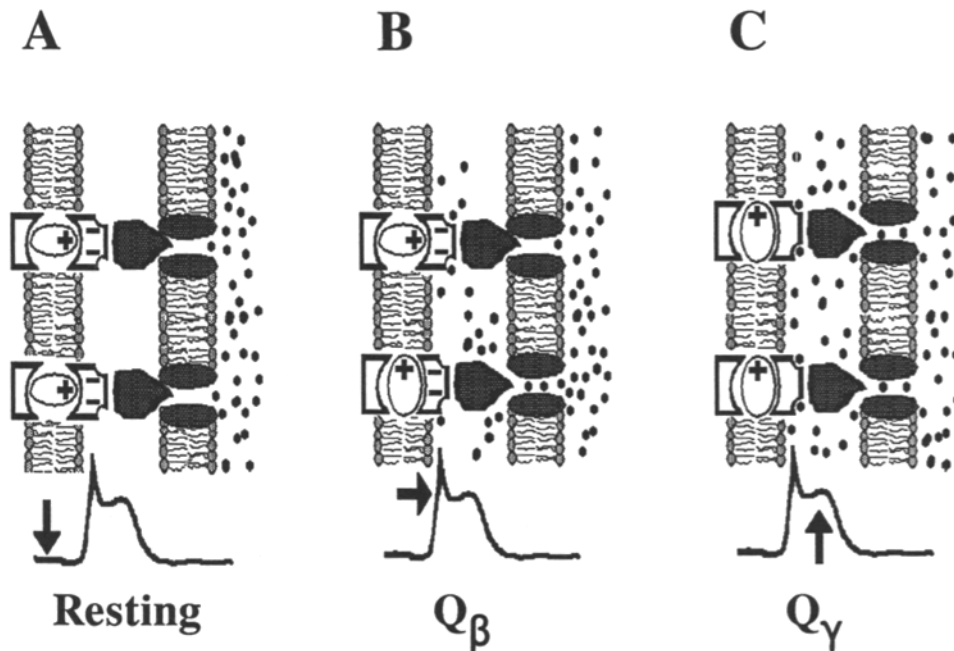

FIGURE 20.   The Ca^{2+}-binding model of I_γ. A represents the situation at rest; the voltage sensors are in the inactive or *cis* position and the release channels are closed. Negative sites on the inside of the sensors contribute a surface potential that makes the microscopic transmembrane potential difference more negative (the arrows on a record of charge movement current mark the event illustrated in each panel). (B) A suprathreshold depolarization causes some voltage sensors to activate, carrying Q_β as they move. This causes the opening of some channels and the beginning of Ca release; as a consequence, $[Ca^{2+}]$ increases near the binding sites and some sites bind Ca^{2+}. (C) The positive charges offset the negative surface potential and the local transmembrane potential increases beyond the value attained at the beginning of the pulse. This increase drives more charge movement (Q_γ in C).

Two possible mechanisms through which the release process could cause the movement of a delayed charge were suggested by W. K. Chandler (quoted by Horowicz and Schneider, 1981). One in particular explains many of the features of I_γ observed here: Ca^{2+}, at an elevated concentration near the release sites, increases the effective transmembrane potential by binding to negatively charged sites on the myoplasmic face of the T membrane. A diagram (Fig. 20) helps understand this mechanism. It is assumed that the internal surface of the T membrane has sites that bind Ca^{2+} with affinity suitable to be essentially Ca^{2+} free at rest, and largely occupied

when $[Ca^{2+}]$ increases locally during Ca release. Fig. 20 *A* represents the situation at rest, while in *B* a suprathreshold depolarization has been applied and some voltage sensors activate, carrying Q_β as they move. This causes the opening of some channels and the beginning of Ca release, and as a consequence $[Ca^{2+}]$ increases near the binding sites and some sites bind Ca^{2+}. The positive charges change the negative surface potential and the local transmembrane potential increases beyond the value attained at the beginning of the pulse. This increase drives more charge movement (Q_γ in Fig. 20 *C*).

The kinetic aspects of the current I_γ and its relationship with $\dot{R}(t)$ are well accounted for by this interpretation. A detailed quantitative modeling of the relationship is presented in the fourth paper of this series. In the following we give a qualitative account of the relationship, which is organized in three steps.

First, consider the relationship between the local $[Ca^{2+}]_i(t)$ near the sensors (and near the release sites) and the waveform $\dot{R}(t)$ of Ca release flux. This relationship will only be specified with the numerical simulations in the fourth paper; however, simple arguments show that it will be close to a proportionality. Specifically, consider the myoplasm as represented by two compartments in series: a small one (T) next to the triad and a bulk compartment (B). The release flux $\dot{R}(t)$ will first enter compartment T. The net flux from T to B will be proportional to the concentration gradient

$$m_{tb} = ([Ca^{2+}]_t - [Ca^{2+}]_b) P \tag{2}$$

where P is a constant. m_{tb} is related to $\dot{R}(t)$ as follows: If v_t represents the volume of compartment T relative to total myoplasmic volume and $[Ca]_t$ represents its total calcium concentration, then

$$m_{tb} = \dot{R}(t) - v_t d[Ca]_t/dt \tag{3}$$

v_t should be very small. If T is a 0.014-μm gap facing ~67% of the T tubule surface, and if the surface area of T tubules per volume of fiber is 0.22 μm^{-1} (Mobley and Eisenberg, 1975) the volume of T is ≈ 0.002 of the fiber volume. Also, the Ca^{2+} buffering capacity of T is expected to be lower than in the bulk myoplasm (no troponin or SR pump sites). Consequently, the second term in Eq. 3 may be neglected as a first approximation, and $\dot{R}(t)$ substituted for m_{tb} in Eq. 2:

$$\dot{R}(t) = ([Ca^{2+}]_t - [Ca^{2+}]_b) P \tag{4}$$

Therefore, at early times when the release flux is large, the local $[Ca^{2+}]$ will be much greater than the bulk concentration. At these times

$$[Ca^{2+}]_t \approx \dot{R}(t)(1/P) \tag{5}$$

Exactly when the back flow (negative term in Eq. 4) becomes nonnegligible depends on the details of the assumptions. A wide range of assumptions, as well as a distributed diffusional model (Pizarro et al., 1991), all lead to time courses of $[Ca^{2+}]_t$ (t) in agreement with the conclusion above.

The second step is the relationship between local $[Ca^{2+}]$ and microscopic transmembrane potential (V_m). Again as a first approximation, if the hypothetical binding sites have a simple stoichiometry and are rapidly equilibrating and far from

saturation, the local potential will be proportional to $[Ca^{2+}]_t$ and, from Eq. 5, approximately proportional to $R(t)$.

Finally, since $I_\gamma(t)$ is capacitive, it will be given approximately by $C \, dV_m/dt$, where C is the relevant capacitance, linear and nonlinear, affected by the potential change. Thus, from these simplest assumptions, the current $I_\gamma(t)$ is expected to be roughly proportional to $\ddot{R}(t)$, as observed. Linear components in I_γ would be exactly equal to $C_1 \, dV/dt$, where C_1 is the linear capacitance involved. The component arising at intramembranous charges would be expected to lag behind dV_m/dt (and $\ddot{R}(t)$). The simulations in the fourth paper show that the observed properties are well accounted for assuming only nonlinear contributions to I_γ.

In this hypothesis the puzzling negative phase of $I_\gamma(t)$ is a simple consequence of the reduction in release flux after the peak, which determines a similar time course of local $[Ca^{2+}]_i$ and in turn a reduction during the ON of the extra potential due to bound Ca^{2+}.

Other Definitions of Q_γ

Long-term depolarization to -40 mV was shown by Adrian and Peres (1979) to suppress a component of charge movement with sharp voltage dependence and delayed kinetics; consequently, it was proposed as a means to separate Q_γ. This procedure is now believed to inactivate part of Q_β in addition to Q_γ (discussed by Huang, 1989), and is not ideal for the isolation of Q_γ. However, the observation that Q_γ is more sensitive to voltage-dependent inactivation is consistent with the observation presented here, that Q_γ is selectively suppressed by conditioning depolarization. The difference is merely one of interpretation; the observation of Adrian and Peres (1979) has been taken as an indication of the existence of a set of γ sensors, intrinsically more susceptible to voltage-dependent inactivation. Our interpretation instead is that depolarizations (conditioning pulses or long-term changes) have a greater effect on I_γ because they interfere with Ca release.

Finally, I_γ has been separated by its sensitivity to tetracaine. Since this is the method used most often and considered the most reliable, we sought to use tetracaine effects as a reference to understand the other interventions. The result is that a much lower concentration than used in the traditional definition had essentially the same effect as the other interventions on both Ca release flux and charge movement current, including the essential elimination of visible humps. Thus, all four interventions provide a consistent separation of a component of current, which we termed I_γ. This definition cannot be considered equivalent to previous definitions since lower concentrations of tetracaine were used. The effects of greater concentrations of tetracaine are currently under study. At greater concentrations the drug causes progressively greater reductions in Ca release flux and charge movement current, apparently including components other than the hump (Pizarro, Csernoch, Uribe, and Ríos, 1989, and unpublished observations).

Concentration-dependent Aspects of the Effect of RR

Baylor et al. (1989) determined a dissociation constant of binding to hypothetical release sites from measurements of birefringence signals elicited by action potentials in intact fibers injected with RR. Assuming that the birefringence signal is propor-

tional to the second power of Ca release, they determined a dissociation constant (which they termed K_2) of 72 μM at 16.5°C and 22.5 μM at 8°C. The inhibition of the birefringence signal could also be fitted directly by a binding isotherm without assuming nonlinearity. This fit gave a K_1 of 23 μM at 16.5°C and 7.8 μM at 8°C.

In our most detailed experiment (at 13°C) we could fit binding isotherms separately to the concentration dependence of inhibition of current and to the effect of the intrinsic absorbance signal. Baylor and Hollingworth (1987) have argued that the birefringence signal reflects binding of Ca^{2+} to a myoplasmic site. Ríos et al. (1983) found evidence that the intrinsic absorbance change has a similar mechanism. The K_1 of Baylor et al. (23 to 7.8 μM) should thus be compared with our estimate from intrinsic signals (3.85 μM) and their K_2 (72 to 22.5 μM) with our estimate from effects on the current (11.4 μM). Our lower estimates probably reflect a greater sensitivity of the cut fibers to RR, as cut fibers have been found more susceptible than intact fibers to other drugs. In turn this may simply reflect the loss of a myoplasmic component that binds the drugs.[3]

The apparently greater sensitivity to RR of the intrinsic signal is in line with the assumption of Baylor et al. (1989) of a high order relationship between birefringence change and release flux.

RR had a blocking effect on Q_γ and little or no effect on Q_β. This is consistent with the report that subthreshold charge is not modified by the injection of RR in intact fibers (Baylor et al., 1989).

REFERENCES

Adrian, R. H., and W. Almers. 1976. The voltage dependence of membrane capacity. *Journal of Physiology*. 254:317–338.

Adrian, R. H., and A. Peres. 1977. A gating signal for the potassium channel? *Nature*. 267:800–804.

Adrian, R. H., and A. Peres. 1979. Charge movement and membrane capacity in frog muscle. *Journal of Physiology*. 289:83–97.

Antoniu, B., D. H. Kim, M. Morii, and N. Ikemoto. 1985. Inhibitors of Ca^{2+} release from the isolated sarcoplasmic reticulum. I. Ca^{2+} channel blockers. *Biochimica et Biophysica Acta*. 816:9–17.

Barry, N. H., and L. D. Carnay. 1969. Changes in light-scattered by striated muscle during excitation-contraction coupling. *American Journal of Physiology*. 217:1425–1430.

Baylor, S. M., and S. Hollingworth. 1987. Effect of calcium (Ca) buffering by Fura2 on the second component of the intrinsic birefringence signal in frog isolated twitch muscle fibres. *Journal of Physiology*. 344:625–666.

---

[3] Additionally, the measured [RR] is probably an underestimate of average [RR] in the working segment, as the light for the optical measurements is focused to a 250-μm-long slit positioned at the center of the 500-μm fiber segment, and RR is continuously diffusing in from the cut ends.

Baylor, S. M., and S. Hollingworth, and M. W. Marshall. 1989. Effects of intracellular ruthenium red on excitation-contraction coupling in intact frog skeletal muscle fibres, *Journal of Physiology*. 408:617–635.

Baylor, S. M., M. E. Quinta-Ferreira, and C. S. Hui. 1985. Isotropic components of Antipyrylazo III signals from frog skeletal muscle fibers. *In* Calcium in Biological Systems. R. P. Rubin, G. Weiss, and J. W. Putney, Jr., editors. Plenum Publishing Corp., New York. 339–349.

Brum, G., and E. Ríos. 1987. Intramembrane charge movement in frog skeletal muscle fibres: properties of charge 2. *Journal of Physiology*. 387:489–517.

Brum, G., R. Fitts. G. Pizarro, and E. Ríos. 1988a. Voltage sensors of the frog skeletal muscle membrane require calcium to function in excitation-contraction coupling. *Journal of Physiology*. 398:475–505.

Brum, G., E. Ríos, and E. Stefani. 1988b. Effects of extracellular calcium on the calcium movements of excitation contraction coupling in skeletal muscle fibers. (With an appendix by G. Grum, E. Ríos, and M. F. Schneider). *Journal of Physiology*. 398:441–473.

Caputo, C. 1972. The time course of potassium contractures of single muscle fibres. *Journal of Physiology*. 223:483–505.

Carnay, L. D., and W. H. Barry. 1969. Turbidity, birefringence and fluorescence changes in skeletal muscle coincident with the action potential. *Science*. 165:508–609.

Csernoch, L., C. L. H. Huang, G. Szűcs, and L. Kovacs. 1988. Differential effects of tetracaine on charge movements and Ca^{2+} signals in frog skeletal muscle. *Journal of General Physiology* 92:601–612.

Csernoch, L., I. Uribe, M. Rodríguez, G. Pizarro, and E. Ríos. 1989. Q_γ and Ca release flux in skeletal muscle fibers. *Biophysical Journal*. 55:88a (Abstr.)

Delay, M., B. Ribalet, and J. Vergara. 1986. Caffeine potentiation of calcium release in frog skeletal muscle fibres. *Journal of Physiology*. 375:535–559.

Endo, M. 1975. Mechanism of action of caffeine on the sarcoplasmic reticulum of skeletal muscle. *Proceedings of the Japan Academy*. 51:479–484.

Endo, M. 1985. Calcium release from the sarcoplasmic reticulum. *Current Topics in Membranes and Transport*. 25:181–230.

García, J., A. J. Avila-Sakar, and E. Stefani. 1991. Differential effects of ryanodine and tetracaine on charge movement and calcium transients in frog skeletal muscle (*Rana pipiens*). *Journal of Physiology*. In press.

García, J., G. Pizarro, E. Ríos, and E. Stefani. 1991. Effect of the calcium buffer EGTA on the "hump" component of charge movement in skeletal muscle. *Journal of General Physiology*. 97:885–896.

González, A., G. Pizarro, J. Ma, C. Caputo, and E. Ríos. 1990. Effects of 1-alkanols on E-C coupling. *Biophysical Journal*. 57:314a. (Abstr.)

Hill, D. K. 1949. Changes in transparency of muscle during a twitch. *Journal of Physiology*. 108:292–302.

Hollingworth, S., M. W. Marshall, and E. Robson. 1987. The effects of tetracaine on charge movement in fast twitch rat skeletal muscle fibres. *Journal of Physiology*. 421:633–644.

Hollingworth, S., M. W. Marshall, and E. Robson. 1990. The effects of tetracaine on charge movement in fast twitch rat skeletal muscle fibres. *Journal of Physiology*. 421:633–644.

Horowicz, P., and M. F. Schneider. 1981. Membrane charge moved at contraction thesholds in skeletal muscle fibres. *Journal of Physiology*. 314:595–633.

Huang, C. L. H. 1980. Charge movement components in skeletal muscle. *Journal of Physiology*. 304:31–32P.

Huang, C. L. H. 1981. Effects of local anesthetics on the relationship between charge movements and contractile thresholds in frog skeletal muscle. *Journal of Physiology*. 320:381–391.

Huang, C. L. H. 1982. Pharmacological separation of charge movement components in frog skeletal muscle. *Journal of Physiology*. 324:375–387.

Huang, C. L. H. 1989. Intramembrane charge movements in skeletal muscle. *Physiological Reviews*. 68:1197–1247.

Huang, C. L. H., and L. D. Peachey. 1989. The anatomical localization of charge movement components in frog skeletal muscle. *Journal of General Physiology*. 93:565–584.

Hui, C. S. 1983a. Differential properties of two charge components in frog skeletal muscle. *Journal of Physiology*. 337:531–552.

Hui, C. S. 1983b. Pharmacological studies of charge movement in frog skeletal muscle. *Journal of Physiology*. 337:509–529.

Hui, C. S., and W. K. Chandler. 1990. Intramembranous charge movement in frog cut twitch fibers mounted in a double Vaseline-gap chamber. *Journal of General Physiology*. 96:257–297.

Imagawa, T., J. S. Smith, R. Coronado, and K. P. Campbell. 1987. Purified ryanodine receptor from skeletal muscle sarcoplasmic reticulum is the Ca^{2+}-permeable pore of the calcium release channel. *Journal of Biological Chemistry*. 262:16636–16643.

Irving, M., J. Maylie, N. L. Sizto, and W. K. Chandler. 1987. Intrinsic optical and passive electrical properties of cut frog twitch fibers. *Journal of General Physiology*. 89:1–41.

Kovacs, L., E. Ríos, and M. F. Schneider. 1983. Measurement and modification of free calcium transients in frog skeletal muscle fibers by a metallochromic indicator dye. *Journal of Physiology*. 343:161–196.

Kovacs, L., and M. F. Schneider. 1977. Increased optical transparency associated with excitation-contraction coupling voltage clamped cut skeletal muscle fibres. *Nature*. 265:556–560.

Kovacs, L., and G. Szűcs. 1983. Effect of caffeine on intramembrane charge movement and calcium transients in cut skeletal muscle fibres of the frog. *Journal of Physiology*. 341:559–578.

Lai, F. A., H. P. Erickson, E. Rousseau, Q.-Y. Liu, and G. Meissner. 1988. Purification and reconstitution of the calcium release channel from skeletal muscle. *Nature*. 331:315–319.

Lamb, G. 1986. Components of charge movement in rabbit skeletal muscle: the effects of tetracaine and nifedipine. *Journal of Physiology*. 376:85–100.

Ma, J., M. Fill, C. M. Knudson, K. P. Campbell, and R. Coronado. 1988. Ryanodine receptor of skeletal muscle is a gap junction-type channel. *Science*. 242:99–102.

Melzer, W., E. Ríos, and M. F. Schneider. 1987. A general procedure for determining calcium release in skeletal muscle fibers. *Biophysical Journal*. 51:849–864.

Melzer, W., E. Rios, and M. F. Schneider. 1984. Time course of calcium release and removal in skeletal muscle fibers. *Biophysical Journal*. 45:637–641.

Melzer, W., M. F. Schneider, B. Simon, and G. Szűcs. 1986. Intramembrane charge movement and Ca release in frog skeletal muscle. *Journal of Physiology*. 373:481–511.

Miyamoto, H., and E. Racker. 1982. Mechanism of calcium release from skeletal sarcoplasmic reticulum. *Journal of Membrane Biology*. 66:193–201.

Mobley, B. A., and B. R. Eisenberg. 1975. Sizes of components in frog skeletal muscle measured by methods of stereology. *Journal of General Physiology*. 66:31–45.

Ohnishi, T. S. 1979. Calcium-induced calcium release from fragmented sarcoplasmic reticulum. *Journal of Biochemistry*. 86:1147–1150.

Pessah, I. N., A. O. Francini, D. J. Scales, A. L. Waterhouse, and J. E. Casida. 1986. Calcium-ryanodine receptor complex. *Journal of Biological Chemistry*. 261:8643–8648.

Pizarro, G., L. Csernoch, I. Uribe, and E. Ríos. 1989. Tetracaine and pathways of Ca^{2+} release in skeletal muscle. *Biophysical Journal.* 55:237a. (Abstr.)

Pizarro, G., L. Csernoch, I. Uribe, M. Rodríguez, and E. Ríos. 1991. The relationship between Q_γ and Ca release from the sarcoplasmic reticulum in skeletal muscle. *Journal of General Physiology.* 97:913–947.

Ríos, E., G. Brum, G. Pizarro, and M. Rodríguez. 1990. Effects of intracellular Ca buffers on Ca transients in skeletal muscle. *Biophysical Journal.* 57:341a. (Abstr.)

Rios, E., W. Melzer, and M. F. Schneider. 1983. An intrinsic optical signal is related to the calcium transient of frog skeletal muscle. *Biophysical Journal.* 41:396a. (Abstr.)

Ríos, E., and M. F. Schneider. 1981. Stoichiometry of the reactions of calcium with the metallochromic indicator dyes Antipyrylazo III and Arsenazo III. *Biophysical Journal.* 36:607-621.

Schneider, M. F., and W. K. Chandler. 1973. Voltage dependent charge movement in skeletal muscle: a possible step in excitation-contraction coupling. *Nature.* 242:244–246.

Schneider, M. F., and B. J. Simon. 1988. Inactivation of calcium release from the sarcoplasmic reticulum in frog skeletal muscle. *Journal of Physiology.* 405:727–745.

Schneider, M. F., B. J. Simon, and G. Szûcs. 1987. Depletion of calcium from the sarcoplasmic reticulum during calcium release in frog skeletal muscle. *Journal of Physiology.* 392:167–192.

Simon, B. J., M. G. Klein, and M. F. Schneider. 1989. Caffeine slows turn-off of calcium release in voltage clamped skeletal muscle fibers. *Biophysical Journal.* 55:793–797.

Sizto, N. L. 1982. Sodium gating current and sodium current in frog twitch muscle fibres. *Biophysical Journal.* 37:69a (Abstr.)

Smith, J. S., R. Coronado, and G. Meissner. 1985. Sarcoplasmic reticulum contains adenine nucleotide-activated calcium channels. *Nature.* 316:446–450.

Szûcs, G., L. Csernoch, J. Magyar, and L. Kovács. 1991. Contraction threshold and the "hump" component of charge movement in frog skeletal muscle. *Journal of General Physiology.* 97:897–911.

Vergara, J., and M. Cahalan. 1978. Charge movement in a cut skeletal muscle fiber. *Biophysical Journal.* 21:167a. (Abstr.)

Vergara, J., and C. Caputo. 1983. Effects of tetracaine on charge movements and calcium signals in frog skeletal muscle fibers. *Proceedings of the National Academy of Sciences, USA.* 80:1477–1481.

Volpe, P., G. Salviati, and A. Chu. 1986. Calcium-gated calcium channels in sarcoplasmic reticulum of rabbit skinned skeletal muscle fibers. *Journal of General Physiology.* 87:289–303.

Xu, L., K. Anderson, and G. Meissner. 1990. Regulation of sarcoplasmic reticulum Ca^{2+} release channel activity. *Biophysical Journal.* 57:400a. (Abstr.)